5-31-1993

Aluminum epitaxy on silicon

Samuel Cruz Ramac
New Jersey Institute of Technology

ABSTRACT

Aluminum Epitaxy on Silicon
by
Samuel Cruz Ramac

The purpose of this work was to study the effect of 4° miscut and chemical pretreatment of Si(111) wafers on the epitaxial growth of Al by thermal evaporation in a UHV environment ($\sim 10^{-9}$ Torr). Two chemical pretreatments of the wafers were used. One included HF only and the other included NH_4F after an initial HF treatment. The substrates were not heated during deposition. XRD measurements of the films were done before and after annealing in a high vacuum oven for one hour at temperatures between 200 and 350°C.

The Al(200) films deposited on wafers pretreated with NH_4F have good quality as indicated by the narrow peaks in the XRD measurements. The peaks narrowed by almost 15% after annealing at temperature as low as 250°C.

The surprisingly good crystallinity and orientation of these films were attributed to the uniformly distributed atomic steps formed on the substrate surface by the chemical pretreatment of NH_4F.

The film deposition work and analytical studies were done at NJIT's Drexler Microelectronics Laboratory and AT&T Bell Laboratories respectively.

ALUMINUM EPITAXY ON SILICON

by

Samuel Cruz Ramac

A Thesis
Submitted to the Faculty of
New Jersey Institute of Technology
in Partial Fulfillment of the Requirement for the Degree of
Master of Science in Electrical Engineering

Department of Electrical and Computer Engineering

May 1993

APPROVAL PAGE

Aluminum Epitaxy on Silicon

Samuel C. Ramac

April 30, 1993

Dr. Marek Sosnowski, Thesis Advisor (date)
Associate Professor of Electrical Engineering, NJIT

May 10, 1993

Dr. Roy Cornely, Committee Member (date)
Professor of Electrical Engineering, NJIT
Director of Surface Modification Center

May 6, 1993

Dr. Haim Grebel, Committee Member (date)
Associate Professor of Electrical Engineering, NJIT

BIOGRAPHICAL SKETCH

Author: Samuel C. Ramac

Degree: Master of Science in Electrical Engineering

Date: May 1993

Date of Birth:

Place of Birth:

Undergraduate and Graduate Education:

- Master of Science in Electrical Engineering,
  New Jersey Institute of Technology, Newark, NJ
  1993
- Bachelor of Science in Electrical Engineering,
  New Jersey Institute of Technology, Newark, NJ
  1991

Major: Electrical Engineering

This thesis is dedicated to my grandmother,
Emiliana M. Cruz

ACKNOWLEDGMENT

The author wishes to express his sincere gratitude to his supervisor, Professor Marek Sosnowski, for his guidance, friendship, and moral support throughout this research.

Special thanks to Dr. Walter Brown of AT&T Bell Laboratories at Murray Hill NJ for his guidance and support.

The author appreciates the kindness of Mr. Matthew Marcus of AT&T Bell Laboratories for letting me use his X-ray diffractometer.

TABLE OF CONTENTS

Chapter	Page
1 INTRODUCTION	1
2 EXPERIMENTAL PROCEDURES	4
2.1 Background	4
2.2 Description of The UHV system	6
2.3 Chemical Treatment of Silicon Wafers	11
2.4 Deposition of Aluminum Films	13
2.5 Annealing of Aluminum Films	15
2.6 Characterization of Aluminum Films	16
2.6.1 Rutherford Backscattering Spectrometry	16
2.6.2 X-ray Diffraction Technique	20
2.6.3 Transmission Electron Microscopy	22
3 EXPERIMENTAL RESULTS	24
3.1 RBS Measurements	24
3.2 XRD Measurements	25
4 DISCUSSION OF RESULTS	44
4.1 RBS Data	44
4.2 XRD Data	45
4.3 TEM Data	52
5 SUMMARY OF RESEARCH FINDINGS	60
BIBLIOGRAPHY	63

LIST OF TABLES

Table		Page
2.1	Typical values of the current and voltage of the source	15
3.1	Thickness of the samples	39
3.2	XRD Measurements of samples cleaned with Process II and annealed sequentially	40
3.3	Wafer cleaned with Process II and annealed only once	41
3.4	XRD measurements of wafer cleaned with Process I	42
3.5	2θ values of Al(100) and Al(111)	43

LIST OF FIGURES

Figure		Page
2.1	Schematic diagram of the UHV system at NJIT	7
2.2	Schematic diagram of the effusion cell	9
2.3	Schematic diagram of the RBS system	18
2.4	RUMP generated RBS spectrum of a 500 Å aluminum film	19
2.5	RUMP generated RBS spectrum of a 1 μm thick aluminum film	20
2.6	X-ray Diffractometer configuration	23
3.1	Example of a RBS spectra showing aluminum film on silicon substrate	27
3.2	Channeling on aluminum	28
3.3	θ scan of Si(111) before annealing	29
3.4	θ scan of Al(200) before annealing	30
3.5	$\theta - 2\theta$ of Al(200) before annealing	31
3.6	θ scan of Al(111) before annealing	32
3.7	$\theta - 2\theta$ scan of Al(111) before annealing	33
3.8	θ scan of Si(111) after annealing	34
3.9	θ scan of Al(200) after annealing	35
3.10	$\theta - 2\theta$ scan of Al(200) after annealing	36
3.11	θ scan of Al(111) after annealing	37
3.12	$\theta - 2\theta$ scan of Al(111) after annealing	38

Figure **Page**

4.1 Comparison between RBS measured thickness and the $\cos^n\theta$ function 46

4.2 Vector notation of the different planes of the film 48

4.3 Vector notation of the different planes Si(111) with the different axes labeled 49

4.4 Illustration of the three possible orientations of Al(100) on Si(111) surface 51

4.5 Schematic diagram of the steps on the Si(111) surface 53

4.6 FWHM vs thickness of Al(200) film for various annealing temperature 54

4.7 Ratio of Al(200) to Al(111) intensity vs annealing temperatures 55

4.8 X-ray intensity vs thickness of Al(200) 56

4.9 Average α versus annealing temperatures 57

4.10 Average 2θ and interplanar spacing vs annealing temperatures 58

4.11 Cross-sectional TEM image. Courtesy of Dr. Young Kim, Bell Laboratories. 59

CHAPTER 1

INTRODUCTION

In the semiconductor industry aluminum and aluminum-based films, because of their low resistivity, are used extensively for the interconnections between contacts on devices and between devices and the outside world. The films used in the devices are not pure aluminum but Al-Cu or Al-Cu-Si alloys. Pure aluminum is not used because of its interaction with silicon which leads to "spiking" and most importantly, its electromigration problems.

Electromigration in Al have been the subject of a lot of studies and research. In the studies performed by d'Heurle and Ames [5], it was shown that electromigration- induced open circuits in polycrystalline aluminum thin film conductors is caused predominantly by diffusion along grain boundaries. It was also shown that a change in the grain size along the length of the conductor line changed its material transport properties [9].

Therefore, to learn more about the mechanism of electromigration, samples with well defined crystal orientation and directions of grain boundaries are highly desirable.

The structure of an aluminum film can be controlled by epitaxial growth on a crystalline substrate with atomically clean surface. In this study pure aluminum was grown epitaxially on Si(111) by thermal evaporation. Despite different crystallographic structures and a large mismatch between the lattice

constants of Si and Al (25%), epitaxial growth of Al(111) on Si(111) has been observed [3] [2][12] [10] [15]. Attempts to grow Al epitaxially in Si(100) have also been made although with less success [6].

The growth of epitaxial films requires a very clean environment which can be achieved in an ultrahigh vacuum (UHV) system. The UHV system used in this study and the experimental procedure used to deposit aluminum films in it are described in Sections 2.2 and 2.3, respectively.

Critical to epitaxial film deposition is the preparation of the substrate surface. The Si(111) wafers used in this study were prepared using the chemical treatment described in reference [7]. The chemical treatment of the Si wafers is the most critical part of this study. The chemical treatment of the wafers as well as the analysis of the composition and the crystal structure of the films were done at AT&T Bell Laboratories in Murray Hill NJ. The analytical techniques used in this study are described in Section 2.6. These analytical techniques include the Rutherford Backscattering (RBS) and channeling, Transmission Electron Microscopy (TEM), and X-ray Diffractometry (XRD). The results of the various measurements are given in Chapter 3.

In this study, the crystal structure of the deposited Al films on Si(111) substrate was totally unexpected. Despite reports in a number of publications [3] [10] [2] [12] that Al(111) films grow on a Si(111) substrate, well oriented Al(200) films were obtained in this work. Moreover, annealing of these films at a relatively low temperature of 250°C further improved the quality of the

films which seem to be nearly single crystals over large areas.

The surprising result has been attributed to the existence of an ordered array of steps on the silicon surface. These steps exists because of the intentional "miscut" of the surface at an angle of about 4° with respect to the Si(111) plane and due to the chemical treatment used to clean and passivate the Si(111) surface [7].

The results obtained in this study are significant on two counts. First, they contribute to the fundamental knowledge of the epitaxial growth of crystals with large lattice mismatch. Second, they may provide the well controlled grain structure desired for model studies of electromigration.

CHAPTER 2

EXPERIMENTAL PROCEDURES

2.1 Background

In order to grow film using thermal evaporation, vacuum system is required. Vacuum system provides the required clean environments for thin film deposition. Under vacuum, the density of gas molecules is very low. This low gas-density environment limits the density of the impurities or contaminants inside the chamber.

Vacuum environment may be characterized by the following parameters: the mean free path of molecules λ_{mfp}, impingement rate ϕ, and the time to form a monolayer t. The mean free path is the average distance a molecule will transverse before colliding with any other molecules.

In high vacuum, λ_{mfp} depends on pressure according to the following equation [13]:

$$\lambda_{mfp} = \frac{kT}{\sqrt{2}\pi P d^2}$$

where k is Boltzmann's gas constant, T the temperature in degrees Kelvin, P is the pressure, and d the molecular diameter.

For example, the λ_{mfp} of air molecules in a 10^{-6} Torr pressure is 50 m while λ_{mfp} is 50 μm in 1 Torr pressure.

At a pressure of 1×10^{-6} Torr which is typical of a high vacuum system, molecules travel in straight lines colliding mostly with the chamber walls rather than with other molecules. Such a condition is called the molecular flow and is desired for depositions of thin films by evaporation.

The impingement rate ϕ defines the number of molecules bombarding a unit surface area in a unit time.

$$\phi = 3.51 \times 10^{22} [\frac{P_{Torr}}{\sqrt{MT}}]$$

P_{Torr} is the pressure in Torr, M is the molecular weight, and T is the gas temperature in Kelvin. The unit for ϕ is [$cm^{-1} \times sec^{-1}$] [13].

The monolayer time, t, is the time required to form a monolayer of molecules on a gas-free surface assuming that every particle arriving at this surface remains bonded to it. The monolayer time is

$$t = \frac{N_s}{\phi}$$

where N_s is the number of molecules per unit area [13].

For example, the time required to form a monolayer of oxygen at pressures of 1, 10^{-6}, and 10^{-10} Torr are 2 μ sec, 2.43 sec, and 6 hours respectively.

From the examples given above, it is clear that in high vacuum (P $\sim 10 \times 10^{-6}$ Torr) λ_{mfp} is much larger than the dimensions of a practical deposition system and therefore the condition of molecular flow is satisfied. The pressure inside a high vacuum system, however, is still too high to assure purity of deposited film since the molecular flow of the film is much lower than the

time required to form a monolayer of the film from the vapor ($\sim$ 1 sec). For deposition of high purity film ultra high vacuum (UHV) is required.

2.2 Description of The UHV system

The ultrahigh vacuum system used in this study was designed and built at the Drexler Microelectronics Laboratory at NJIT. Components of the system were bought from different manufacturers and then assembled at NJIT. The author was involved in the design and assembly of the whole system as a part of the thesis work. The schematic of the UHV system is shown in Figure 2.1.

The main chamber from UHV Instruments has a volume of 100 liters. It is made of 1/4-in. thick stainless steel cylindrical chamber 90 cm high and 41 cm wide. It has 29 flanges of various sizes, all sealed with copper gaskets.

The system has a load-lock chamber in the form of a cross with six flanges which is attached to one of the 8-in. flanges of the main chamber with a gate valve in between. An ionization gauge, a turbomolecular pump, a sample loading device, and a door are attached to the remaining sides of the cross. The load-lock system is capable to transfer 5-in. wafer to the main chamber.

A window was installed on the main chamber near the load lock in order to view the loading of the wafer.

A structure for handling and manipulating 5-in. wafers used for depositions was designed and built as a part of this thesis work (Figure 2.2). The wafer is held in a horizontal plane by 3 arm spider-like structure which is

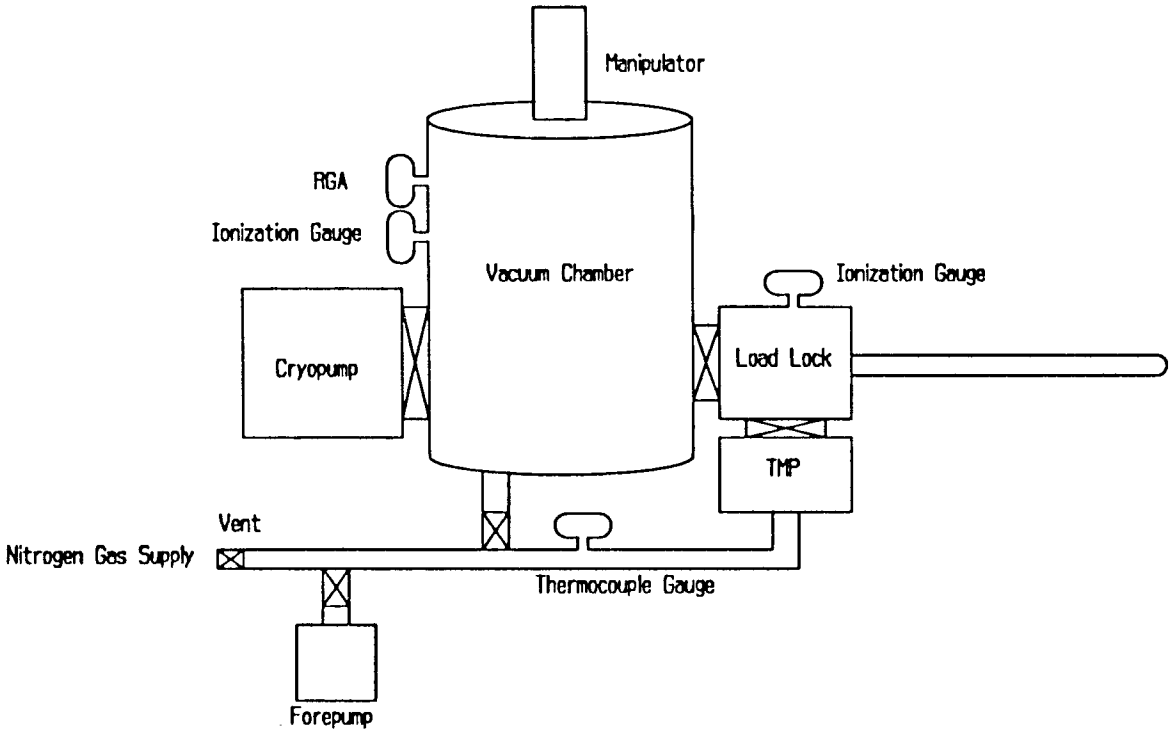

Figure 2.1: Schematic diagram of the UHV system at NJIT

connected to the manipulator vertical shaft. The wafer can then be rotated to any angle as well as moved up and down ($\pm$ 1 inch) and sideways (tilt and translation). Just below the wafer is a stainless steel shield with a sector opening. This shield masks most of the wafer and allows depositions only on the exposed area. Depositions on five different sectors is possible by turning the manipulator shaft 72° between depositions.

To monitor the deposition rate a water cooled bakeable crystal quartz deposition rate monitor (Inficon Inc.) was installed. The monitor controller (Inficon XMS-3 Thin Film Deposition Controller) provides a digital readout of the rate in [Å/sec] and an integrated deposited film thickness.

The deposition source mounted on the bottom flange of the chamber is an effusion cell made at AT&T Bell Laboratories. It contains a 5.08-cm high pyrolytic boron nitride crucible with an ID = 1.016 cm. and OD = 1.143 cm. The opening of the crucible is approximately 17.78 cm. below the wafer. A thermocouple (W-3% Re vs W-25% Re) measures the temperature of the bottom of the BN crucible. The effusion cell is surrounded by a cylindrical stainless steel water cooled shield which prevents heat radiation from heating the interiors of the chamber. Two shutters were installed above the effusion cell. One shutter covers the cell opening and the other covers the quartz monitor and the sector hole.

One of the problems with the the present configuration of the system is that the sector opening of the shield is not on the axis of the crucible. This

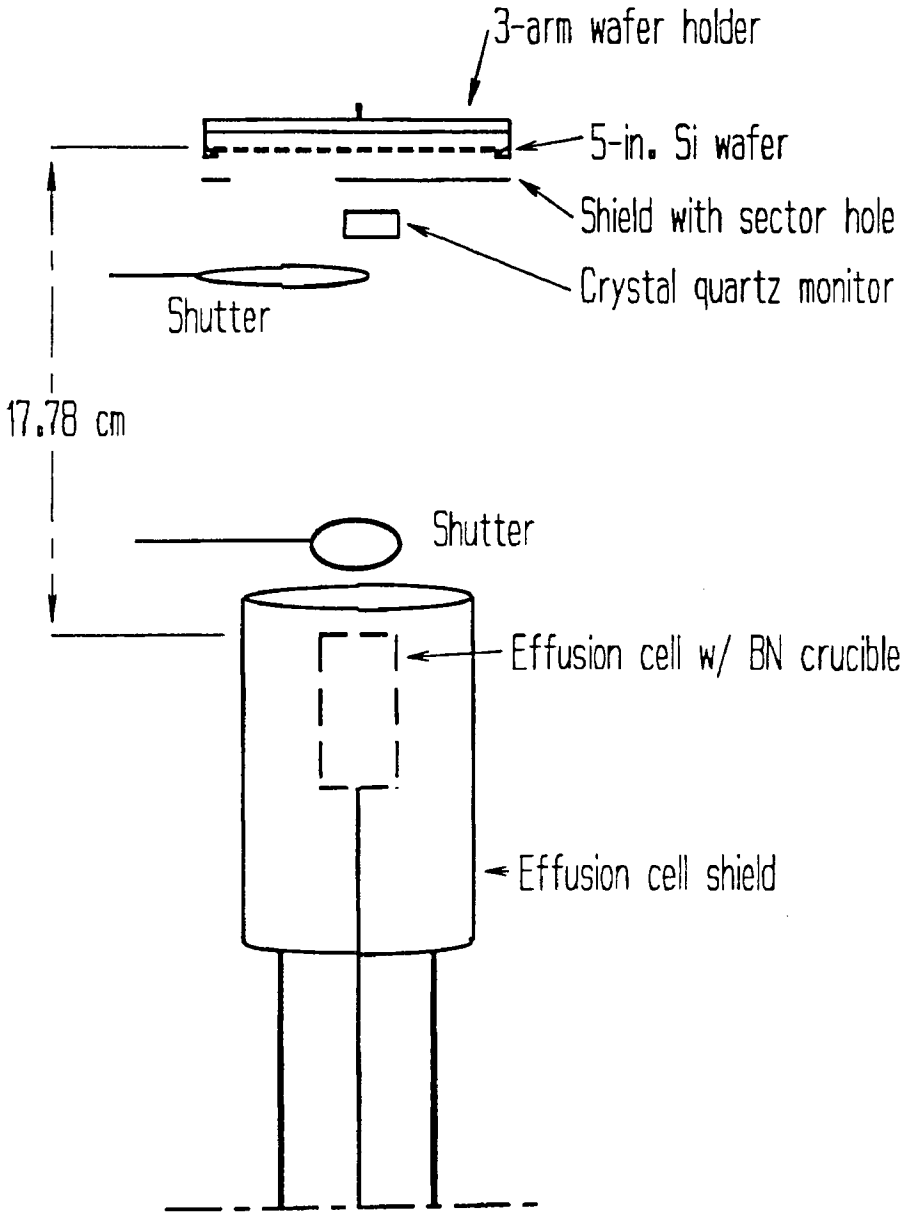

Figure 2.2: Schematic diagram of the effusion cell

results in an increased in non-uniformity in the thickness of the deposited film.

The system uses three different pumps: a CTI-Cryogenics 8" cryogenic pump, a Leybold-Heraeus (LH) Turbovac turbomolecular pump (TMP-150), and a LH Trivac mechanical pump. The mechanical pump is used as the forepump of the turbomolecular pump and the cryogenic pump is used to bring down the pressure inside the main chamber down to the ultrahigh vacuum. The turbomolecular pump brings down the pressure inside the load lock chamber down to 10^{-7} Torr. It also isolates the main chamber from the mechanical pump during the initial pumping preventing any oil vapor from the MP from streaming up to the main chamber. For the same purpose, a molecular sieve filter has been installed in the fore vacuum line between the mechanical and the turbomolecular pumps. All the pumps are isolated from the main system with gate valves made by High Vacuum Apparatus Mfg. Co.

The pressure inside the system is monitored by two ionization gauges which are connected to a Granville-Phillips GP 303 Vacuum Process Controller. One of the gauges measures the vacuum inside the main chamber and the other measures the pressure inside the load lock chamber. A Quadrex 200 Residual Gas Analyzer monitors the gas composition in the main chamber.

The UHV system is vented with nitrogen gas from a high pressure cylinder. A 5-psi check valve was installed in the venting line to prevent over

pressure of nitrogen when venting.

To obtain ultrahigh vacuum in a reasonable time the chamber has to be baked. During the baking process the chamber is subjected to elevated temperatures ($< 200\,^{\circ}C$) which degasses the inside surface and structures of the system. The system was usually baked for approximately 4–5 days using four 3-ampere heating tapes for a total power of 1440 Watts. Two days after baking the pressure inside the chamber was in the 10^{-10} Torr range. The readings using Bayard-Alpert type ionization gauge (Granville-Phillips Model 274-023 Thoria coated filaments) of 1.2–1.8 $\times 10^{-10}$ Torr were obtained routinely.

2.3 Chemical Treatment of Silicon Wafers

Before depositing Al on silicon wafers, the wafers were chemically cleaned by following one of the two processes given below.

PROCESS I

1. The wafer was submerged in a 5:1 solution of $H_2SO_4 : H_2O_2$.
2. The wafer was rinsed in hot deionized water at $105\,^{\circ}C$.
3. The wafer was rinsed in cold deionized water.
4. The wafer was submerged in a 100:1 HF solution for about 2 minutes.
5. The wafer was rinsed in cold deionized water.

6. The wafer was spin dried.

PROCESS II

1. The wafer was submerged in a 5:1 solution of $H_2SO_4 : H_2O_2$.
2. The wafer was rinsed in hot deionized water at 105 °C.
3. The wafer was rinsed in cold deionized water.
4. The wafer was submerged in a 100:1 HF solution for about 2 minutes.
5. The wafer was rinsed in cold deionized water.
6. The wafer was submerged in NH_4F for 2 minutes.
7. The wafer was rinsed in cold deionized water.
8. The wafer was spin dried.

All the chemicals including water used in the chemical cleaning were of very high (semiconductor grade) purity. Only the wafer to be used in deposition is cleaned.

The main difference between Process I and Process II is that in Process II the wafer was submerged in an ammonium fluoride (NH_4F) solution after step 5.

Step 1 in each process oxidizes Si while Step 4 dissolves the oxidized layer. The combination of this two steps removes the contaminated surface

of silicon wafer exposing clean silicon. Silicon surface is quickly oxidized upon exposure to air. However, submerging the wafer in HF and NH_4F passivates the silicon surface with hydrogen atoms i.e. Hydrogen atoms are attached to the dangling bonds of silicon thus preventing oxidation. NH_4F also etches certain silicon crystallographic orientations preferentially therefore leaving flat and evenly distributed steps [7].

2.4 Deposition of Aluminum Films

The chemical treatment of the Si wafers was carried out at AT&T Bell Laboratories and then a clean sample was brought to the NJIT laboratory within 2 hours after cleaning. The HF treatment prevented the surface of wafers from oxidizing. At NJIT, the wafer was then transferred to the the load-lock chamber of the UHV system using a Teflon tweezer. During the transfer to the load-lock chamber, nitrogen gas from the venting system was blowing through the load-lock door to prevent air and particularly water vapor from entering the system. The door of the load-lock chamber was open for only a short time, approximately 1 minute.

Once the wafer was on the sample loading device inside the load-lock chamber the turbomolecular pump was turned on and the chamber was evacuated. While the wafer was inside the load-lock chamber the ionization gauge was turned off to prevent emissions from the gauge filament from contaminating the wafer. After 20 minutes the wafer was transferred to the the

main chamber where it rested on the 3 arm "spider" structure.

To start the Al deposition the power to the effusion cell heater was turned on and the voltage was gradually increased. The power supply was set to voltage controlled mode. Using the voltage vs the temperature table of the effusion cell thermocouple the voltage to the cell was steadily increased until the temperature reached 500 °C. From then on the temperature was increased very slowly as it approached the melting point of aluminum (660 °C). The phase transition at the aluminum melting point may cause severe stresses on BN crucible and even cracking. The same care was taken during cooling cycle of the crucible.

When the voltage was 25 volts and the current was 4.91 ampere the deposition rate was approximately equal to 1 [Å/sec]. At this deposition rate the shutters were opened and the first deposition was started. The deposition rate was controlled by regulating the crucible temperature which in turn depended on the effusion cell current and voltage. Typical values are given in Table 2.1.

When the desired film thickness was obtained the shutter to the sector hole was closed and the wafer was turned 72 degrees clockwise. The deposition rate controller was also reset at this point and the shutter was opened for the next deposition.

After five depositions, the current to the source was reduced very slowly until the temperature of the BN crucible was less than 550 °C, then the

Table 2.1: Typical values of the current and voltage of the source

Voltage (V)	Current (A)	Temperature (°C)	Deposition Rate Å/sec
4	1.75	12.78	--
5	2.00	21.11	--
6	2.5	48.89	--
10	3.22	107.22	--
12	3.22	348.89	--
13	3.35	432.22	--
14	3.48	476.67	--
16	3.89	593.33	--
18	4.03	698.88	--
20	4.38	732.22	--
23	4.77	826.67	--
24	4.95	904.44	--
25	5.00	926.67	1

current was steadily reduced to 0 A.

2.5 Annealing of Aluminum Films

The Al films were annealed at various temperatures using a Lindbergh high vacuum oven. The samples were annealed in the $1\text{-}2\times10^{-8}$ Torr range pressures for 1 hour. The samples were cleaned before every annealing step using trichloroethane, acetone and methanol in an ultrasonic cleaner for approximately 5 minutes.

The Lindbergh high-vacuum oven is made of a cylindrical crystal quartz with one side inside a hot furnace or hot zone. The sample stays in the

cold zone while pumping-down system which usually takes about 5 minutes. When the desired temperature and pressure ($\sim 1 \times 10^{-8}$ Torr) are reached the samples which are loaded in a crystal quartz boat were inserted into the hot zone. The annealing time was counted from the moment of insertion of the boat with samples in the hot zone.

2.6 Characterization of Aluminum Films

Rutherford Backscattering Spectrometry (RBS) and X-ray Diffractometry (XRD) were the primary techniques used for analyzing the aluminum films deposited on Si(111) and Si(100) substrates. Principles of the two methods are outlined below. Both the RBS and the XRD measurements were done in AT&T Bell Laboratories at Murray Hill, NJ.

2.6.1 Rutherford Backscattering Spectrometry

RBS is a technique where the sample to be analyzed is bombarded with monoenergetic ions (usually He^+) while the energy of the ions scattered at large angles is measured. The schematic diagram of a RBS system is shown in Figure 2.3. Using the laws of conservation of momentum and conservation of energy the mass of the target atoms and therefore the target composition can be obtained from the maximum energy of the scattered ions. RBS is more sensitive in detection of heavy elements than light elements because the scattering probability or scattering cross section is proportional to the

square of the atomic number.

The scattered ions have well defined energy when the target has a form of a very thin film (Figure 2.4). Ions scattered from thick target have a continuous energy distribution with well defined high energy edge determined by the initial ion energy and the target ions (Figure 2.5). Lower energies in the spectrum correspond to the ions scattered beneath the target surface which loose their energy as they pass through a layer of the target material.

This energy loss or the difference between the high and the low energy edge of a spectrum group which corresponds to a given thin film target element can then be used to determine the film thickness. If the film and the substrate elements have close atomic mass numbers there is an overlap of the energy spectra corresponding to the different elements. Overlap in the energy spectrum also occurs when thin films of low atomic mass element is deposited on a light atomic mass substrate.

Interpretation of RBS spectra of Al film on Si substrate is particularly complicated because of the close mass of the two elements (26.98 and 28.04 respectively). The spectra can be calculated from the scattering kinematics and the well known energy loss of He^+ ions in the materials.

Channeling is one of the most important concept related to RBS. Channeling happens when ions traveling in a certain directions go through the film with minimal collisions because the rows and planes of the crystalline materials line up at that direction [14]. Using the concept of channeling,

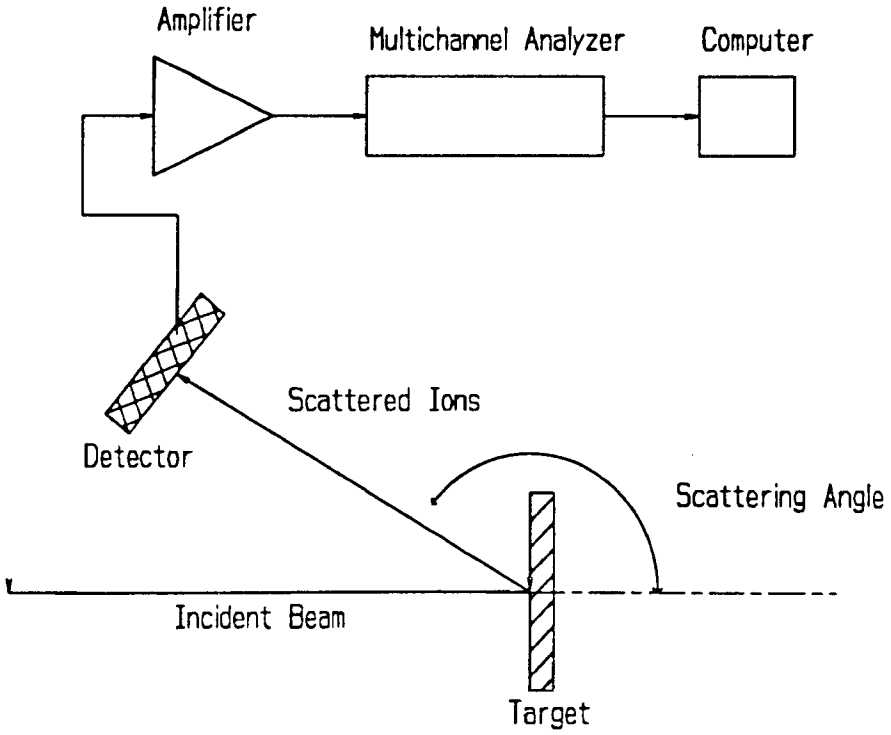

RBS Schematic Diagram

Figure 2.3: Schematic diagram of the RBS system

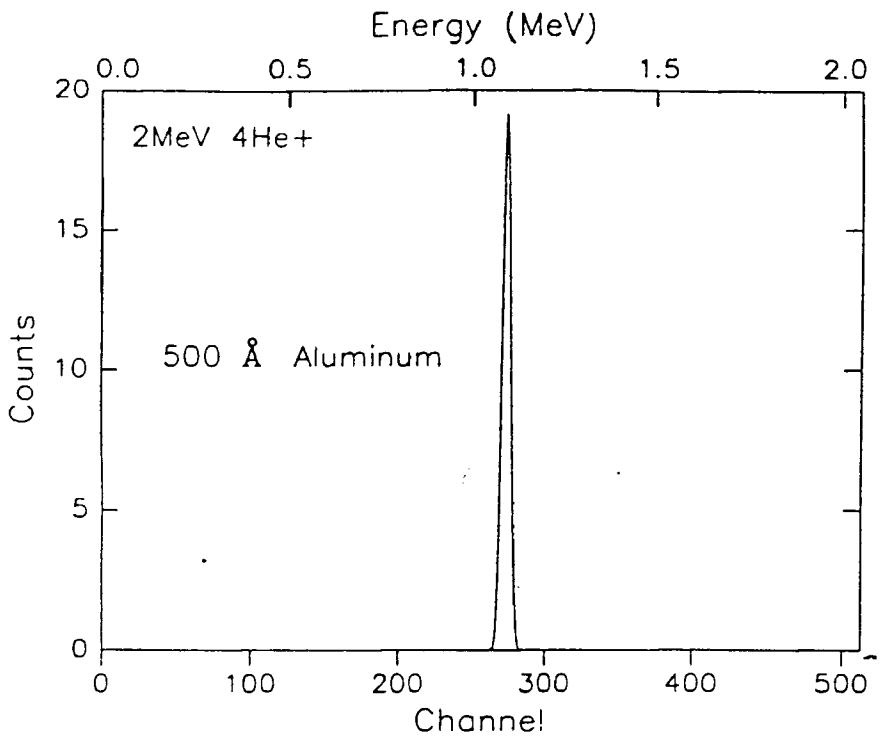

Figure 2.4: RUMP generated RBS spectrum of a 500 Å aluminum film

RBS can be used to study the crystallographic quality and structure of the deposited film.

A RBS simulation program called RUMP was used in this thesis to compare the calculated spectra of a film with that of the experimental results. The program takes account of the scattering kinematics as well as of the energy losses of the ions in the target. Two examples of the RBS spectra obtained with the RUMP program are given in Figures 2.4 (500Åthick sample) and Figure 2.5 (1μm thick sample).

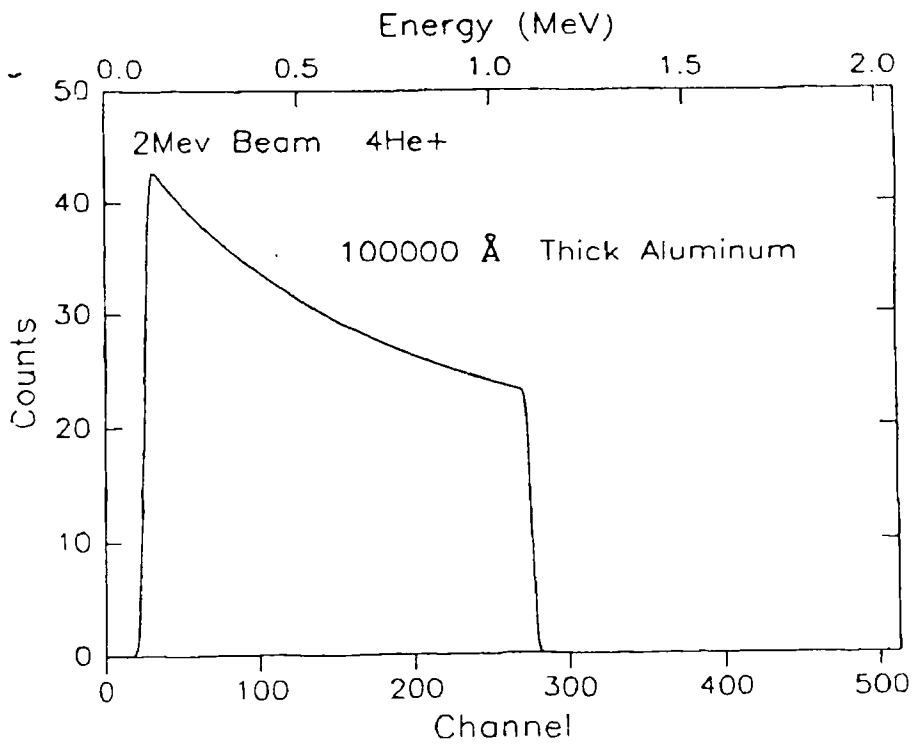

Figure 2.5: RUMP generated RBS spectrum of a 1 μm thick aluminum film

2.6.2 X-ray Diffraction Technique

X-ray Diffraction (XRD), is an analytical technique used to characterize the structure and orientation of crystalline materials. X-ray diffraction is based on the fact that waves with the same wavelengths and phase will interfere constructively producing diffraction. X-ray beams reflected from crystallographic planes are used to characterize crystal structure because wavelengths of x-ray are comparable to the lattice constants of materials. The diffraction condition is given by Bragg's Law which states that

$$n\lambda = 2d \sin \theta$$

where λ is the x-ray wavelength, d is the interplanar spacing, θ is the Bragg's diffraction angle, and n is the diffraction order. Diffraction occurs only if the above equation is satisfied [1].

In a x-ray diffractometer a nearly monochromatic x-ray beam strikes the surface of the sample at an angle θ with the detector at an angle 2θ with respect to the incident beam. The x-ray diffractometer configuration is shown in Figure 2.6.

Two different type of scans were made in this study, θ and $\theta - 2\theta$ scans. In $\theta - 2\theta$ scans the sample is rotated to a different θ settings while the angle 2θ is advanced by double the θ increments[1]. Diffraction maxima appear wherever θ coincides with a Bragg angle. A measure of 2θ is used to identify the interplanar spacing or d of the sample.

In the θ scans, so called rocking curves, the angle θ is increased with 2θ kept constant. θ scans can determine the orientation of the cystallographic planes with respect to the surface of the sample.

XRD measurements can determine the quality of the crystals. For example, mosaic structure crystals versus single crystals can be distinguished from the width of the peaks in θ scans. Single crystal films have low full width half maximum (FWHM) value as the crystal planes have the same orientation. If a crystal is divided into domains with somewhat different orientations the

[1]Note that if the sample crystallographic planes are not parallel to the plane of the diffractometer sample holder then the angle $2\theta \neq 2 \times \theta$. The rocking curve, however can be determined in this case as the 2θ advances in increments double the increments of θ.

θ scan peak becomes broader. If a polycrystalline film consists of randomly oriented crystallites no peak appears in the θ scan. The FWHM of the XRD peak is a function of crystallite size and strain.

Both θ and $\theta - 2\theta$ scans were made on the samples. The primary x-ray diffractometer used was a Siemens D500-K810 with a Cu anode(λ = 1.54060Å) and Ni filter.

2.6.3 Transmission Electron Microscopy

Transmission Electron Microscopy (TEM) is used to obtain structural information from specimens thin enough to transmit electrons. Samples are thinned to thickness of a few thousand angstroms so electron beams can be transmitted through and form diffraction patterns.

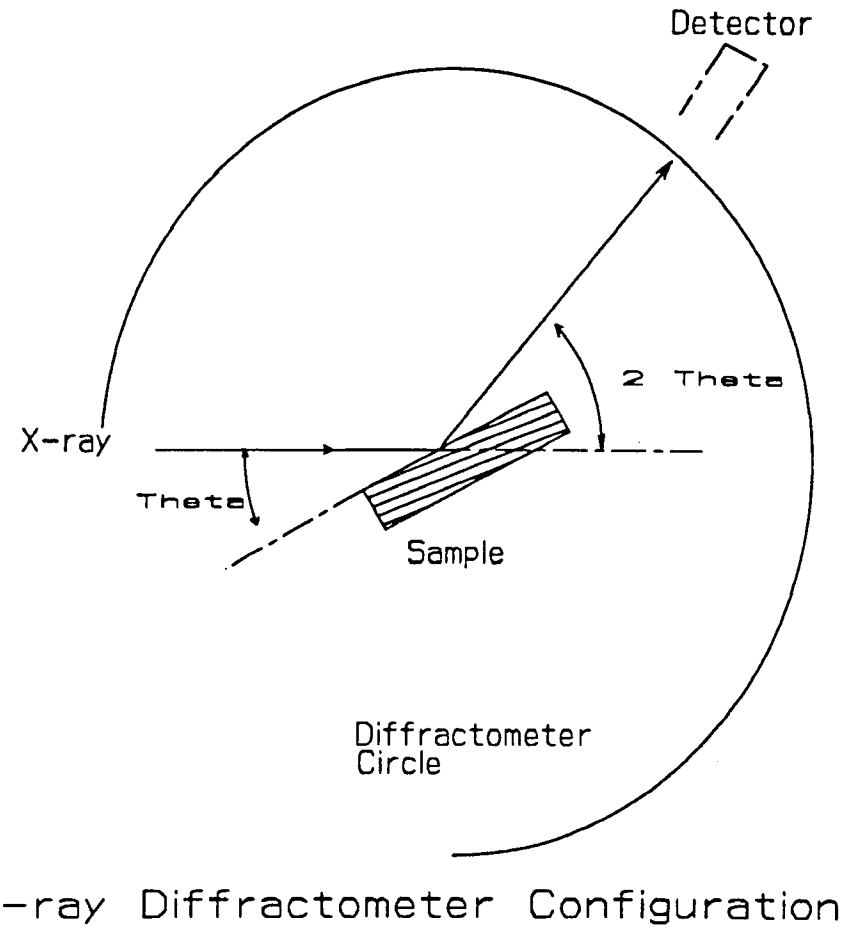

Figure 2.6: X-ray Diffractometer configuration

CHAPTER 3

EXPERIMENTAL RESULTS

In this study, pure aluminum (99.999%) was deposited on six 5-inch wafers (P-type, ρ = 20–30 Ω-cm). Wafers 1–2 were used for the test run of the system. Wafers 3–5 were prepared by using Process II while wafer 6 was prepared using Process I chemical cleaning described in Section 2.3. Besides the chemical treatment received by each wafers, the basic deposition conditions were all the same.

The samples tested with RBS and XRD techniques were taken from various parts of the wafers. The samples are labeled as follows:

$$X - YZa$$

where X is the wafer number, Y is the sector number, and Za is the number of a cut in a given sector (e.g. 5-5a1, wafer 5, sector 5 and cut a1).

3.1 RBS Measurements

RBS measurements in this study, were used to determine the thickness of the deposited aluminum films. An example of the RBS spectra (Sample 5-5 not annealed) is shown in Figure 3.1.

Film thickness in angstrom is given by:

$$\text{thickness} = \Delta\text{channel} \times (84.84\text{Å/channel})$$

where Δchannel is the front edge channel minus back edge channel (Figure 3.1).

A RBS spectrum showing channeling on aluminum is given in Figure 3.2.

3.2 XRD Measurements

XRD measurements were performed on every sample used in this study and they represent the main body of data in this work.

Figures 3.3 – 3.12 show representative plots of θ and $\theta - 2\theta$ scans of sample 5-5. A detailed summary of the plots is given below.

Figure 3.3 is the θ scan of Si(111), Sample 5-5 (not-annealed) while Figure 3.4 and Figure 3.5 are the θ and $\theta - 2\theta$ scans of Al(200), respectively. Figures 3.6 and 3.7 are the θ and $\theta - 2\theta$ scans of Al(111), respectively.

Figure 3.8 is the θ scan of Si(111), Sample 5-5 (annealed at 200 °C and 250 °C). Figures 3.9 and 3.10 are the θ and $\theta - 2\theta$ scans of Al(200), respectively. Figures 3.11 and 3.12 are θ and $\theta - 2\theta$ scans of Al(111), respectively.

In the θ and $\theta - 2\theta$ plots, GENPLOT, a scientific plotting software was used to plot the raw data and generate a fitting curve.

The FWHM and the maximum intensity values of the peaks were calculated from the fitted curve. The curve fitting equation is

$$f(x) = amp(graf * (gaussian) + (1 - gfrac) * (lorentzian))$$

where gaussian and lorentzian have the same FWHM and peak.

Table 3.2 summarizes the results of the XRD measurements of the samples chemically cleaned by following Process II cleaning procedure described in Section 2.3. These samples of various thickness were annealed at different temperatures sequentially starting from 200 °C to 350 °C.The annealing process was described in Section 2.5.

In Table 3.2, the fourth column entitled Ratio of Al(200)/Al(111) is the ratio of the x-ray intensity of Al(200) to Al(111). Dtheta = Position - θ_{ideal}, where Position was obtained from the plot and θ_{ideal} is the bragg diffraction angle. Dtheta therefore, represents the angle between the vector orientation and the surface normal. θ_{ideal} is 19.24°, 22.365°, and 14.22° for Al(111), Al(200), and Si(111) respectively. The Si(111) wafers used in this study have 4° "miscut", this means that the Si(111) planes are at an angle of 4° to the surface normal.

Table 3.3 is the summarizes the results of the XRD measurements of the samples cleaned by following Process II and each annealed at only one temperature (Wafer 5).

Table 3.4 is the summary of the XRD measurements of the samples cleaned by Process I (Wafer 6).

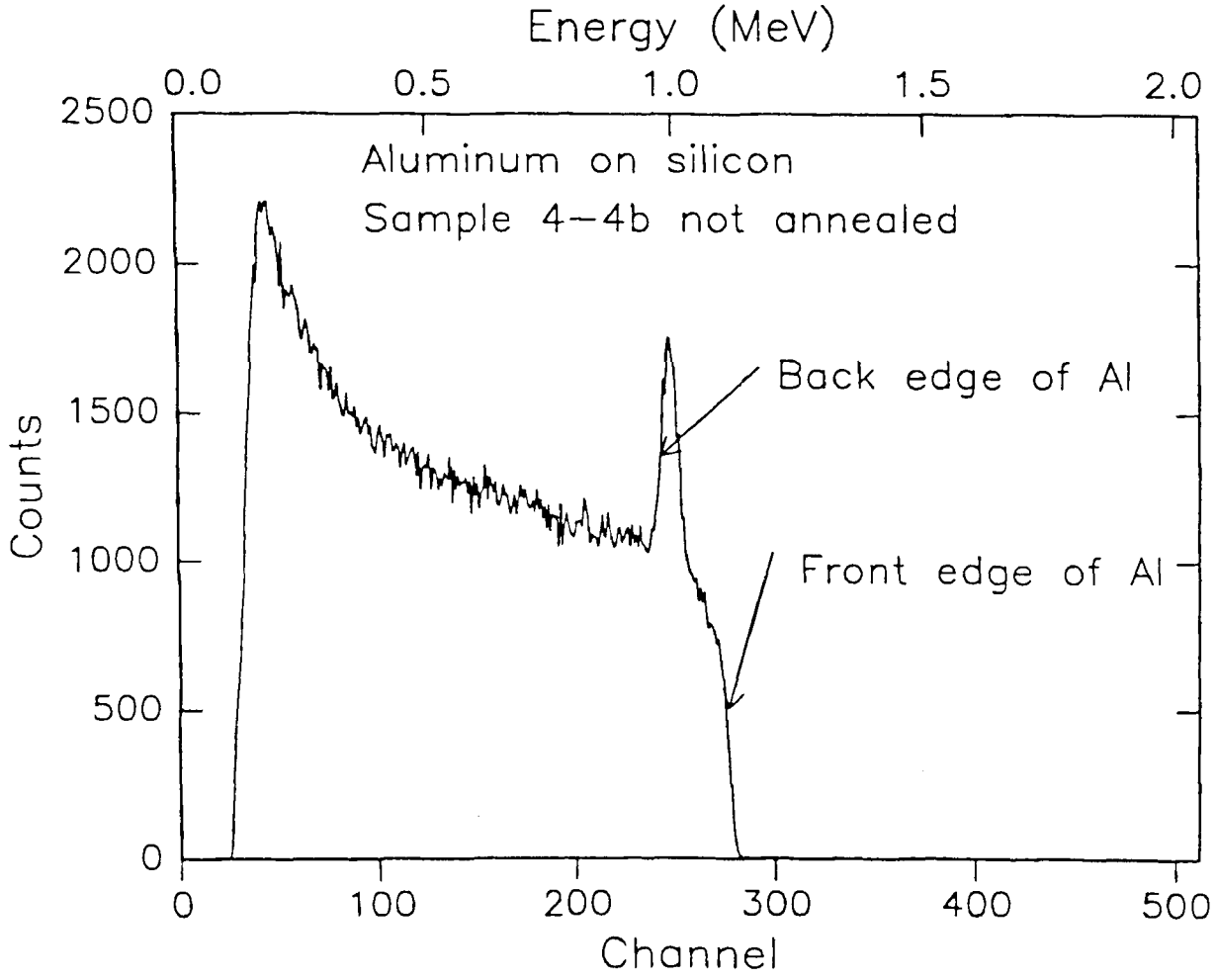

Figure 3.1: Example of a RBS spectra showing aluminum film on silicon substrate

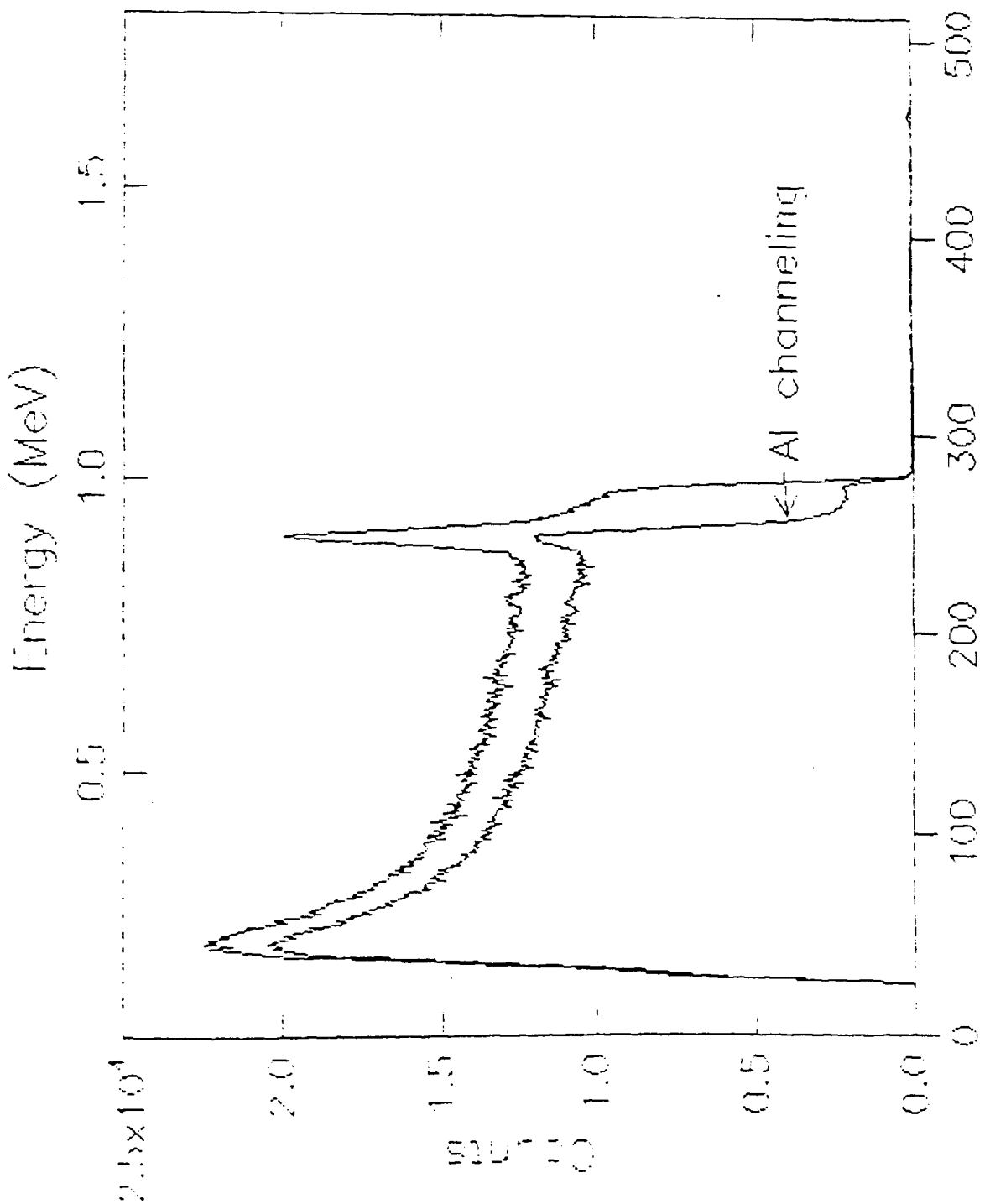

Figure 3.2: Channeling on Aluminum

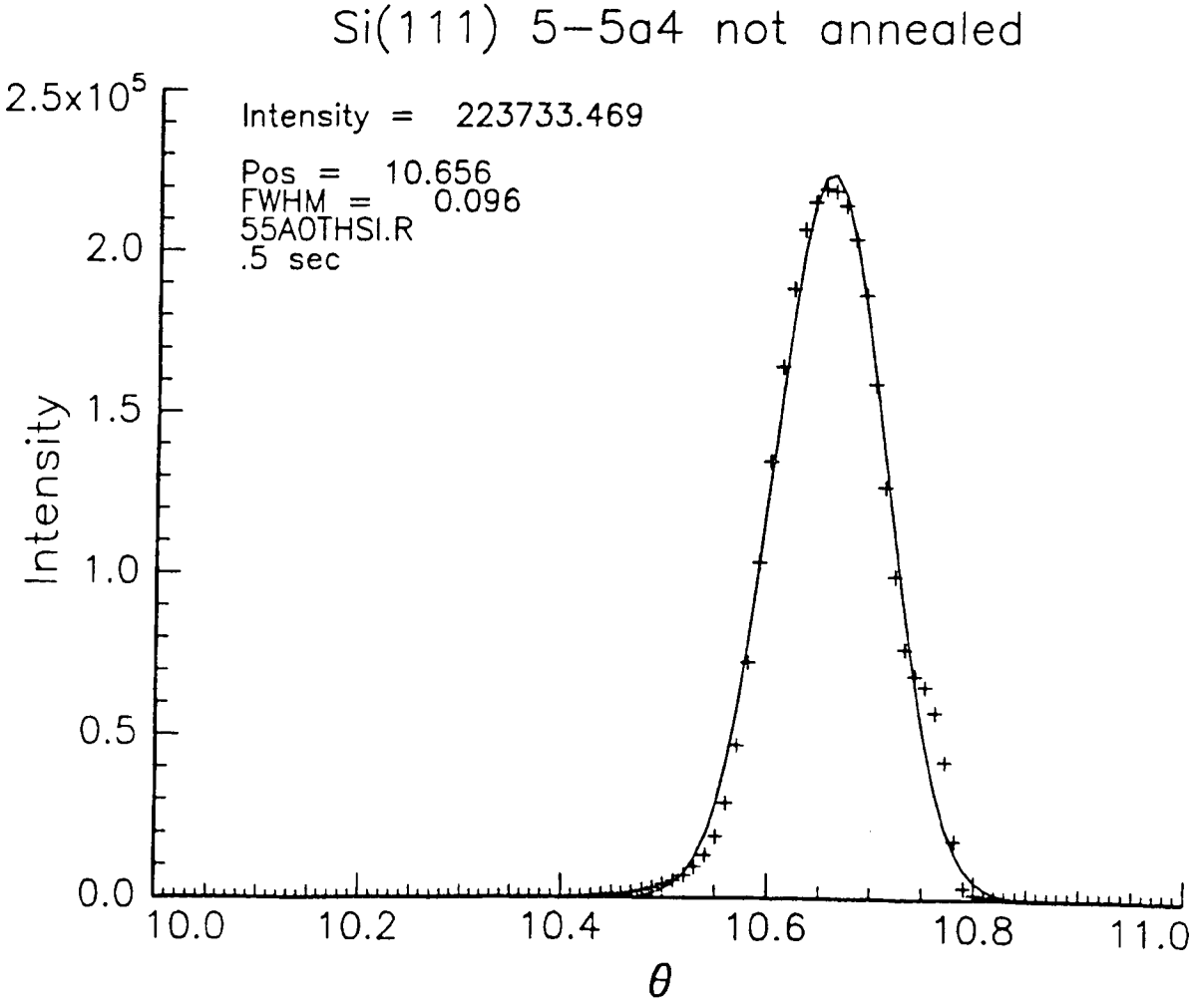

Figure 3.3: θ scan of Si(111) before annealing

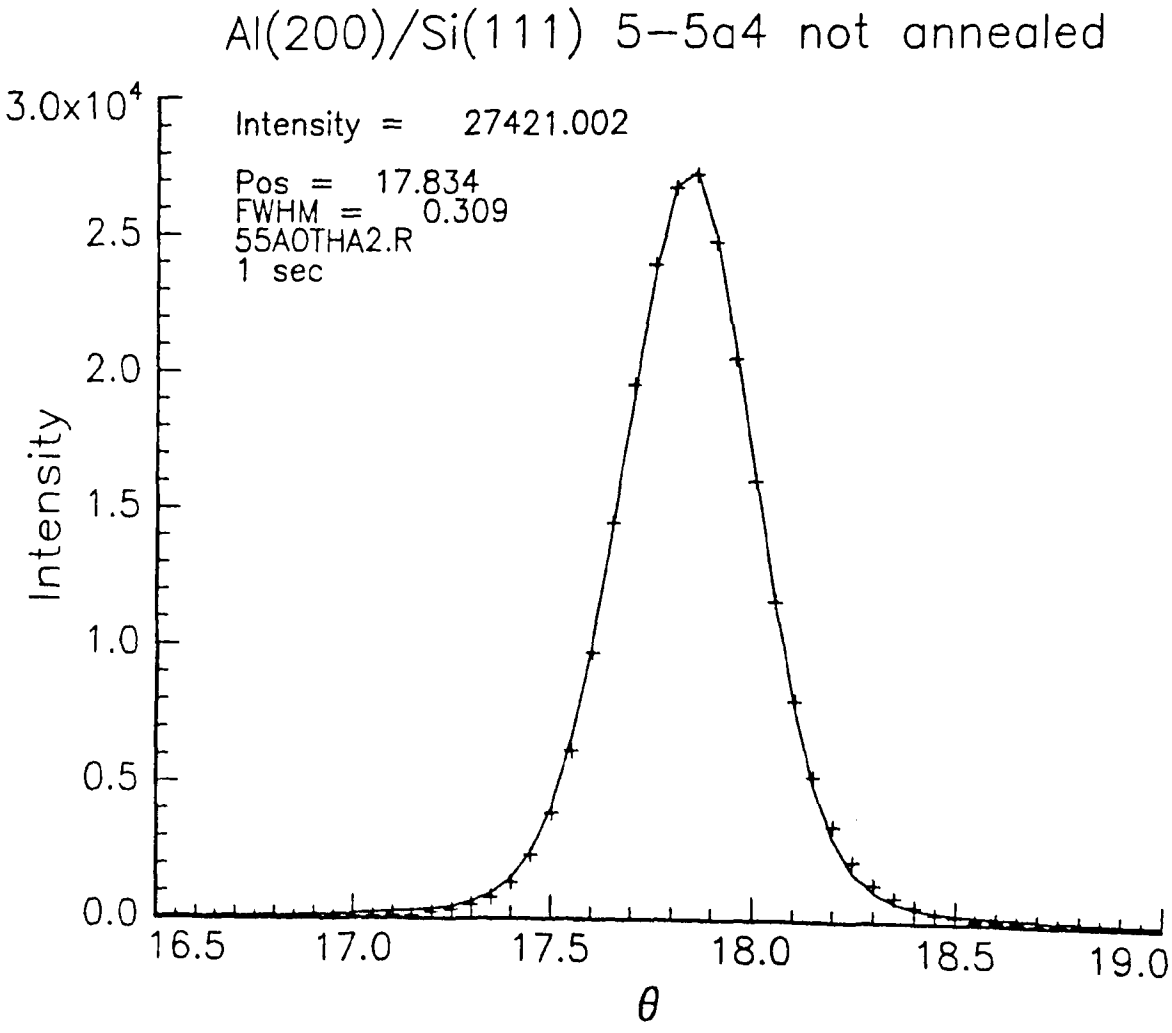

Figure 3.4: θ scan of Al(200) before annealing

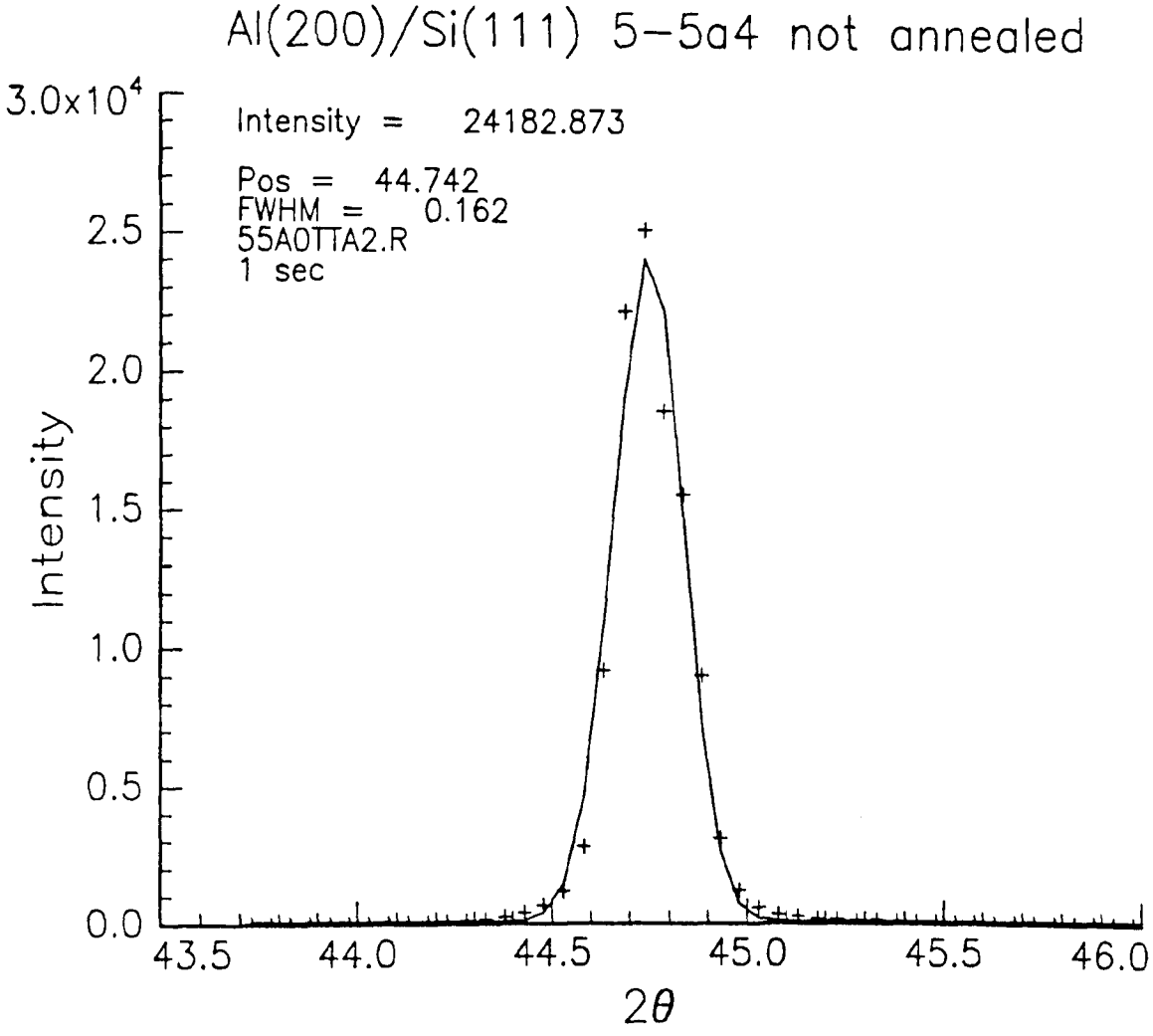

Figure 3.5: $\theta - 2\theta$ of Al(200) before annealing

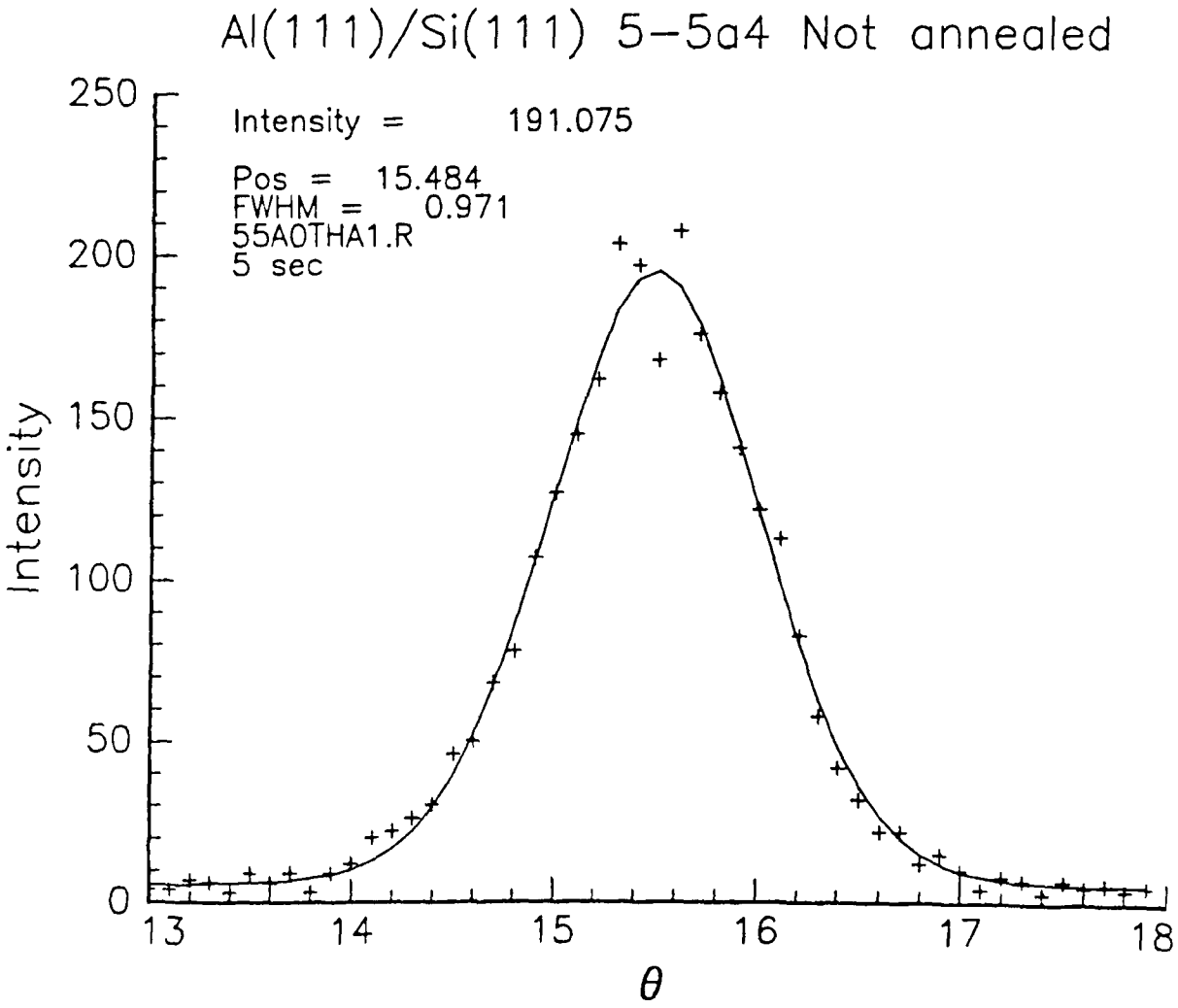

Figure 3.6: θ scan of Al(111) before annealing

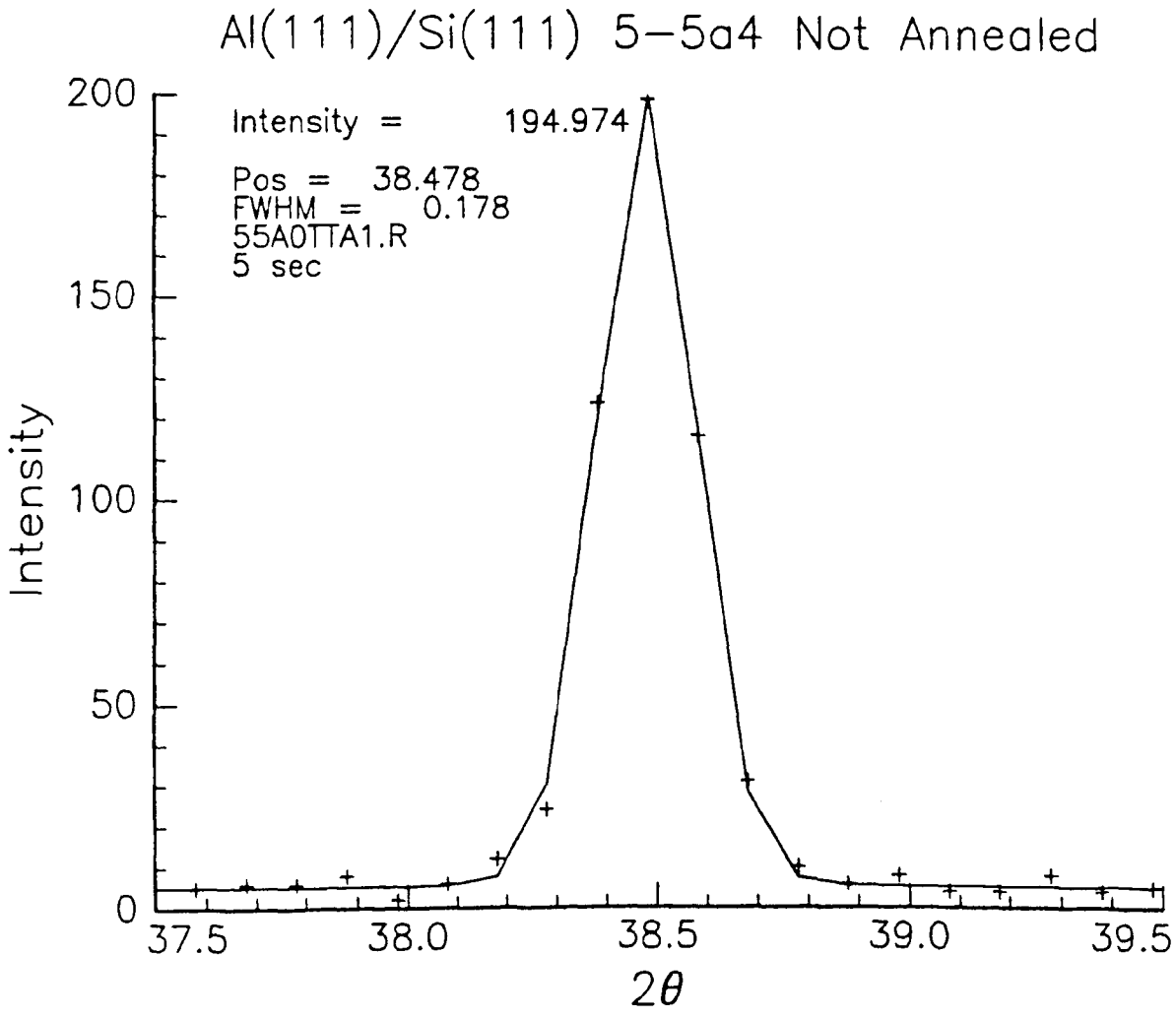

Figure 3.7: $\theta - 2\theta$ scan of Al(111) before annealing

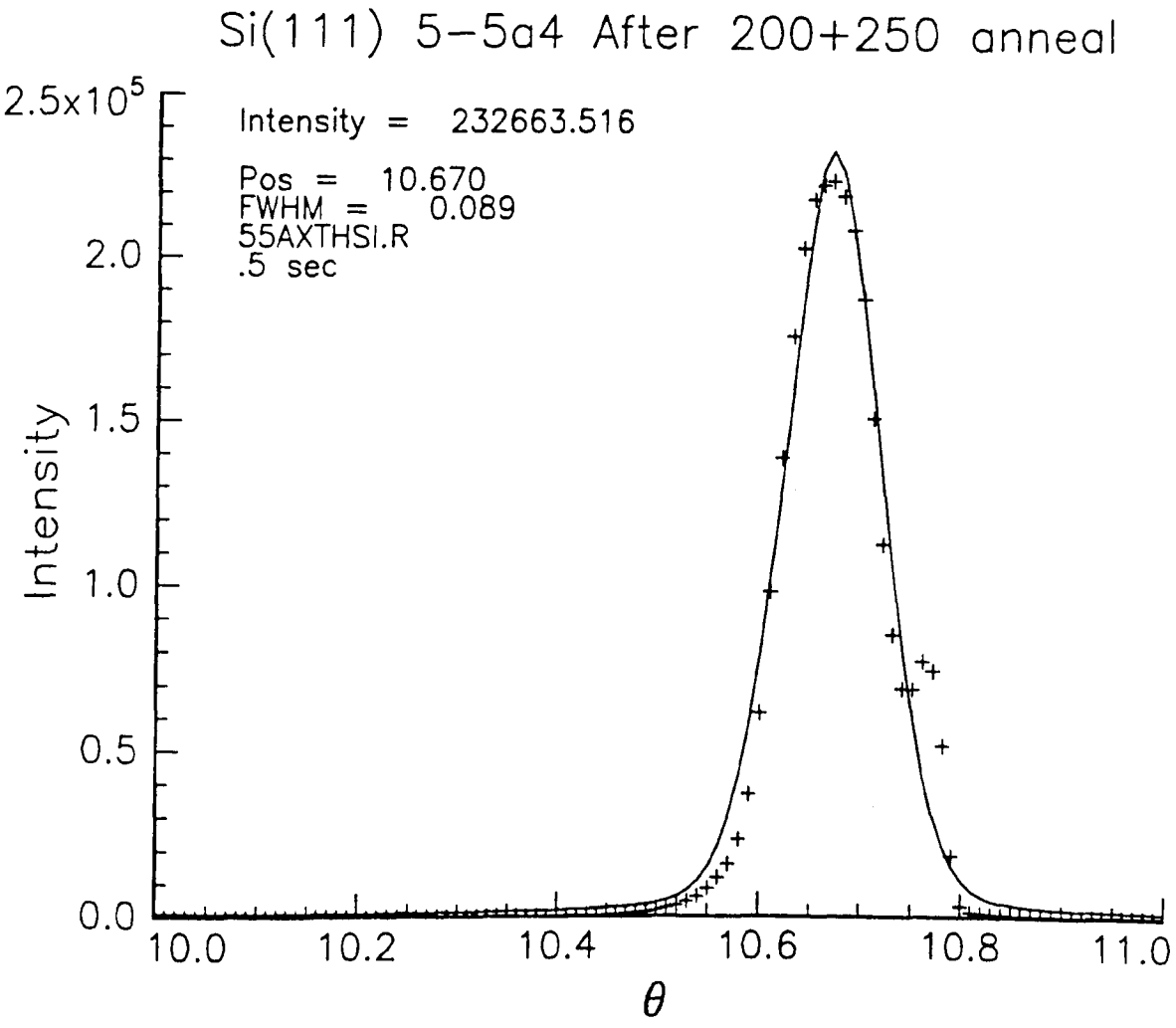

Figure 3.8: θ scan of Si(111) after annealing

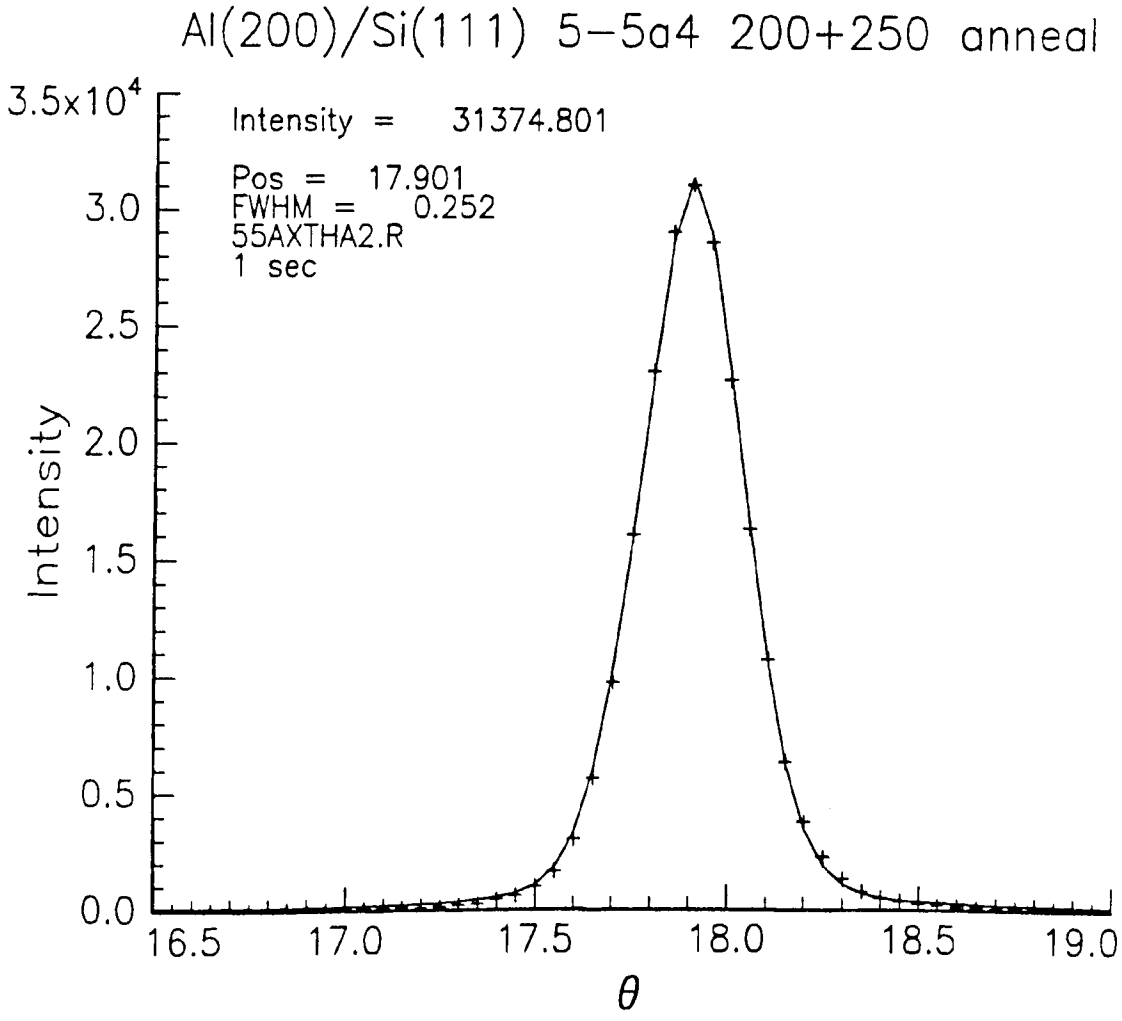

Figure 3.9: θ scan of Al(200) after annealing

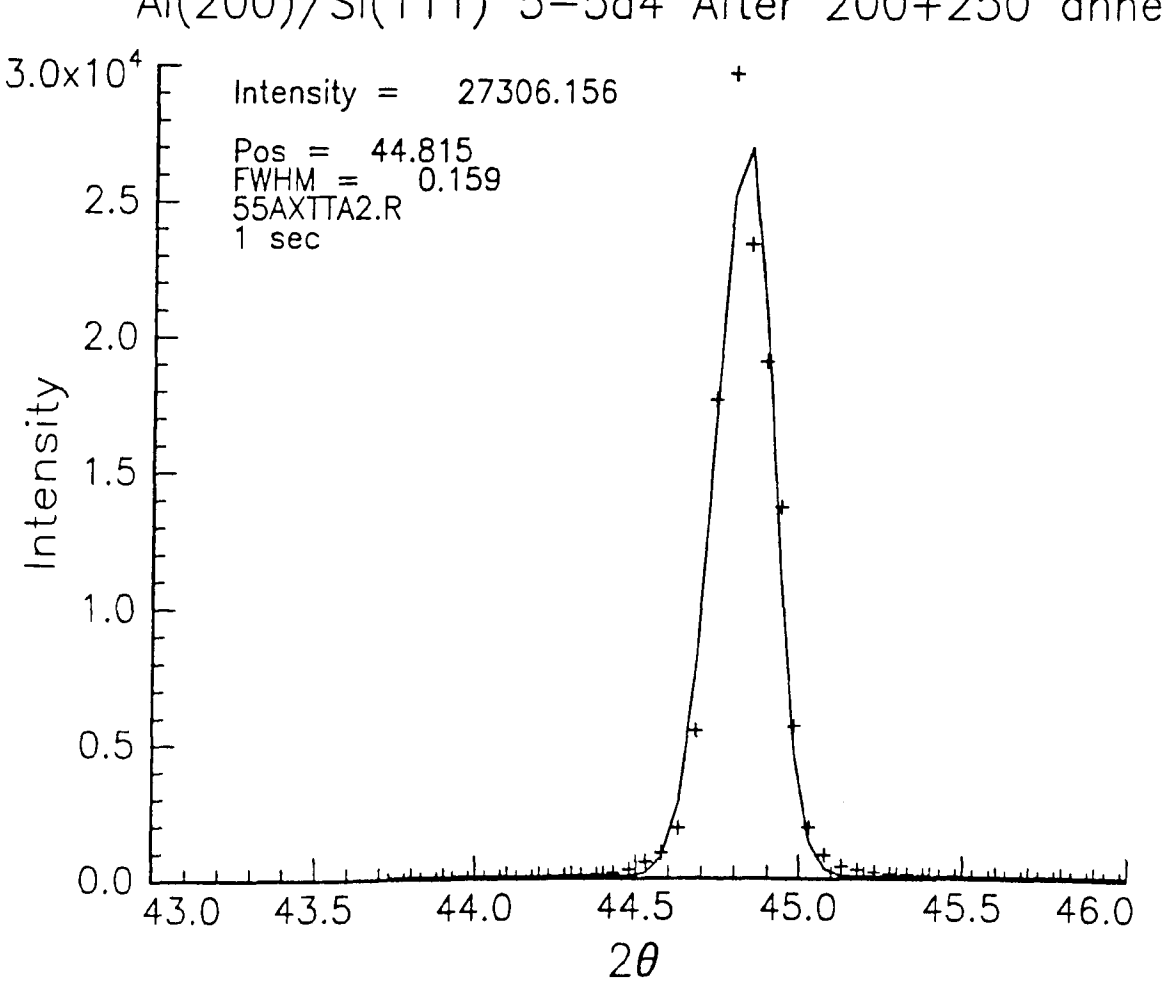

Figure 3.10: $\theta - 2\theta$ scan of Al(200) after annealing

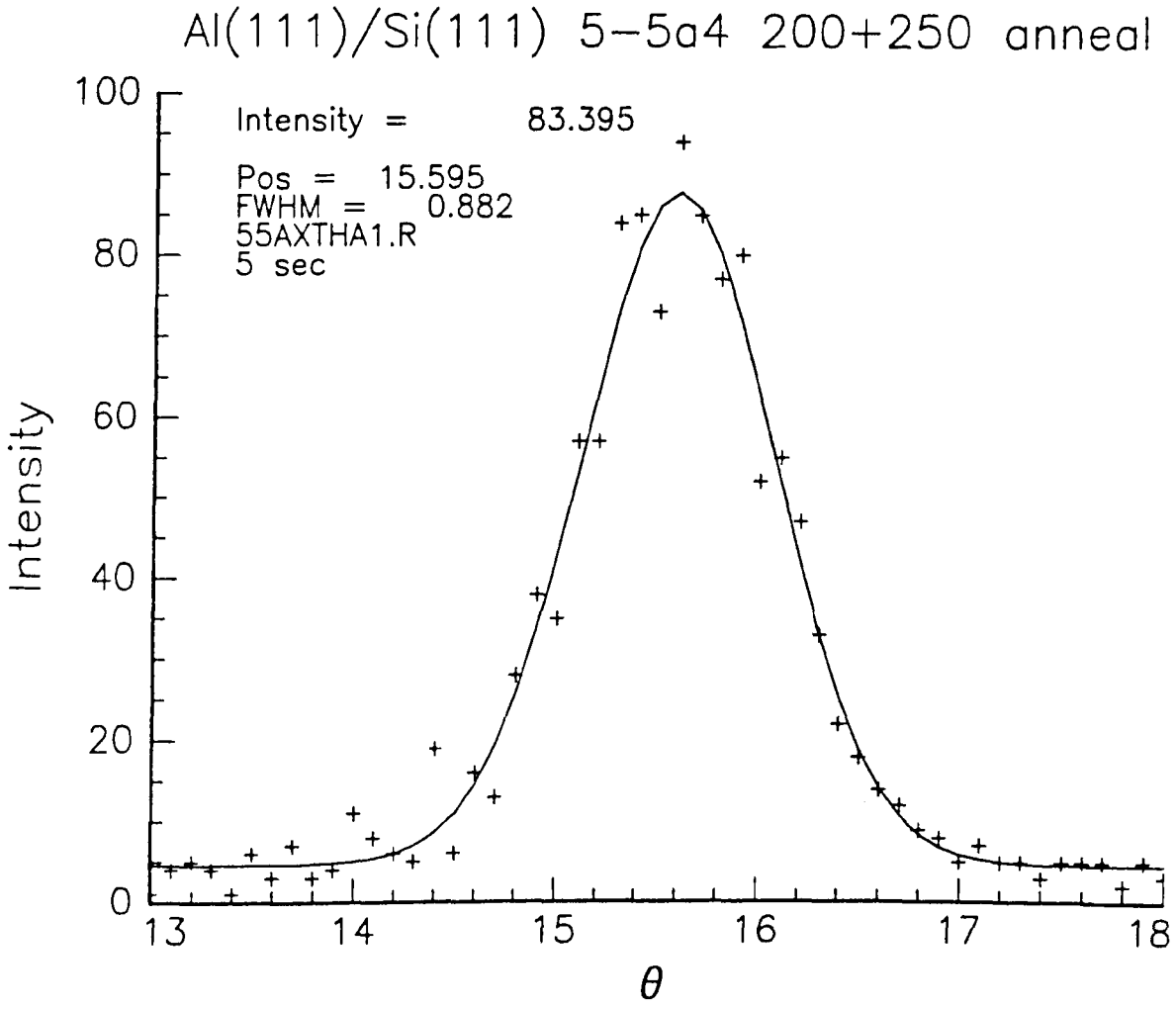

Figure 3.11: θ scan of Al(111) after annealing

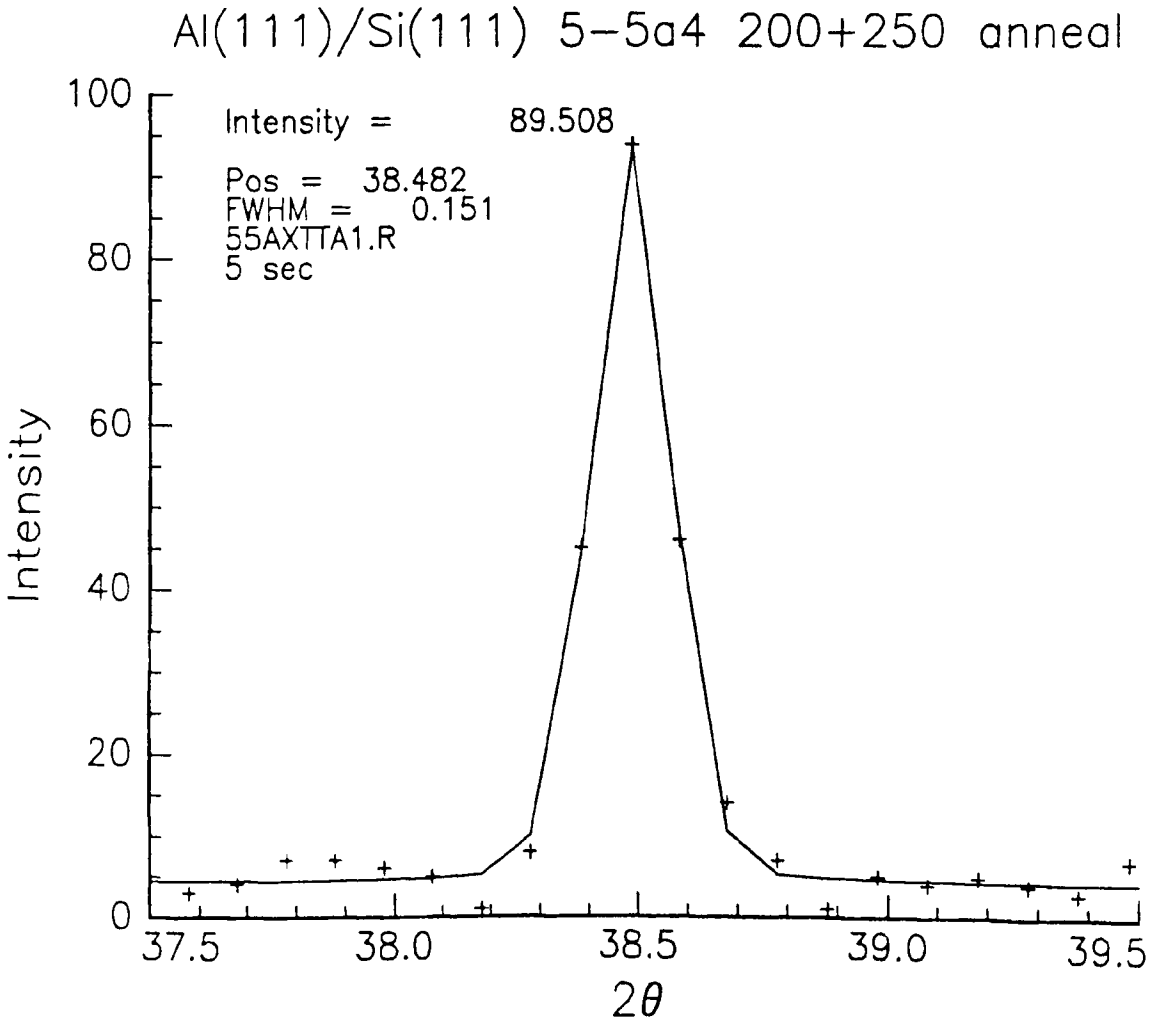

Figure 3.12: $\theta - 2\theta$ scan of Al(111) after annealing

Table 3.1: Thickness of the samples

Sample	Monitor Å	RBS Å
5-2a1	250	116
5-2a2	250	80
5-2a3	250	50
5-2a4	250	42
5-4a1	1000	385
5-4a2	1000	359
5-4a3	1000	312
5-4a4	1000	266
5-1b1	7000	2610
5-1b2	7000	2610
5-1b3	7000	2540
5-1b4	7000	2280
5-5a1	16000	7430
5-5a2	16000	5760
5-5a3	16000	4670
5-5a4	16000	3540

Sample	RBS Thickness (A)	Anneal Temp (C)	Ratio Al(200)/ Al(111)	Al(200) Intensity			Al(111) Intensity			Si(111) Intensity			Al(200) dt-dtsi	Al(111) dt-dtsi
				Dtheta	(cts/sec)	FWHM	Dtheta	(cts/sec)	FWHM	Dtheta	(cts/sec)	FWHM		
5-1B4	2280	RT	580.55	4.563	15702.04	0.300	3.915	27.047	1.002	3.600	445457.5	0.091	0.963	0.315
		200	854.48	4.496	18530.28	0.264	3.859	21.686	0.934	3.566	446888.9	0.095	0.93	0.293
		+250	1472.41	4.389	18363.90	0.233	3.758	12.472	0.923	3.498	446608.3	0.097	0.891	0.26
		+300	2883.35	4.444	15766.13	0.241	3.675	5.468	0.838	3.546	468052.9	0.099	0.898	0.129
		+350	7314.26	4.444	12324.53	0.265	3.675	1.685	1.069	3.519	454045.3	0.100	0.925	0.156
5-2A4	42	RT	2.08	4.385	2.71	1.392	3.571	1.304	2.079	3.539	460994.7	0.095	0.846	0.032
		200	7.88	4.353	10.84	0.982	3.340	1.375	1.795	3.513	462053.7	0.093	0.84	-0.173
		+250	7.31	4.396	11.78	1.223	3.404	1.613	1.842	3.475	451802.3	0.093	0.921	-0.071
		+300	7.83	4.264	15.12	1.062	3.517	1.931	1.505	3.497	452012.7	0.097	0.767	0.02
		+350	5.64	4.160	13.22	1.053	3.605	2.342	1.485	3.490	448513.2	0.097	0.67	0.115
5-4A4	266	RT	24.80	4.438	531.77	0.551	3.546	21.441	1.250	3.479	455865.8	0.087	0.959	0.067
		200	25.11	4.400	541.10	0.532	3.485	21.545	1.178	3.468	445353.3	0.084	0.932	0.017
		+250	38.42	4.447	661.49	0.499	3.639	17.217	1.165	3.533	445433.8	0.088	0.914	0.106
		+300	30.06	4.409	524.60	0.500	3.579	17.450	1.071	3.538	442806.7	0.089	0.871	0.041
		+350	27.65	4.335	524.65	0.485	3.521	18.972	1.021	3.518	436694.6	0.090	0.817	0.003
5-5A4	3540	RT	717.55	4.531	27421.00	0.309	3.756	38.215	0.971	3.564	447466.9	0.096	0.967	0.192
		200	1435.72	4.465	27840.11	0.286	3.692	19.391	0.994	3.517	444067.5	0.091	0.948	0.175
		+250	1881.10	4.464	31374.80	0.252	3.645	16.679	0.882	3.550	465327.0	0.089	0.914	0.095
		+300	20168.15	4.424	33277.45	0.226	3.727	1.650	0.728	3.525	451401.2	0.090	0.899	0.202
		+350	9260.06	4.454	29585.90	0.235	3.515	3.195	0.804	3.520	457680.1	0.095	0.934	-0.005

Table 3.2: XRD Measurements of samples cleaned with Process II

Sample	RBS Thickness (A)	Ratio Al(200)/ Al(111)	Anneal Temp (C)	Al(200) Intensity dtheta	(cts/sec)	FWHM	Al(111) Intensity dtheta	(cts/sec)	FWHM	Si(111) Intensity dtheta	(cts/sec)	FWHM	Al(200) dt-dtsi	A(111) dt-dtsi
5-1B4	2280	580.55	RT	4.563	15702.04	0.3	3.915	27.05	1.002	3.600	445457.5	0.091	0.963	0.315
5-1B1	2610	3352.22	250	4.432	26449.00	0.214	3.82	7.89	0.787	3.521	460585.8	0.099	0.911	0.299
5-1B2	2610	8325.74	300	4.412	27066.97	0.215	3.74	3.25	0.919	3.531	453616.5	0.105	0.881	0.209
5-1B3	2540	3590.45	350	4.444	23614.38	0.226	3.726	6.58	0.795	3.522	465735.8	0.104	0.922	0.204
5-2A4	42	2.08	RT	4.385	2.71	1.392	3.571	1.30	2.079	3.539	460994.7	0.095	0.846	0.032
5-2A2	80	16.84	250	4.484	56.79	0.679	3.414	3.37	1.548	3.521	444184	0.096	0.963	-0.107
5-2A3	50	4.04	300	4.36	31.53	0.808	3.469	7.80	1.397	3.518	459687.8	0.097	0.842	-0.049
5-2A1	116	11.08	350	4.337	91.13	0.661	3.429	8.23	1.152	3.513	458676.5	0.097	0.824	-0.084
5-4A4	266	24.80	RT	4.438	531.77	0.551	3.546	21.44	1.250	3.479	455865.8	0.087	0.959	0.067
5-4A3	312	36.51	250	4.508	931.68	0.448	3.6	25.52	1.159	3.588	462631.2	0.085	0.92	0.012
5-4A2	359	43.35	300	4.528	1273.84	0.407	3.653	29.39	1.031	3.652	432638.3	0.09	0.876	0.001
5-4A1	385	59.01	350	4.339	1399.44	0.382	3.503	23.72	0.926	3.518	419953.4	0.099	0.821	-0.015
5-5A4	3540	717.55	RT	4.531	27421.00	0.309	3.756	38.22	0.971	3.564	447466.9	0.096	0.967	0.192
5-5A3	4670	3084.62	250	4.455	49286.00	0.226	3.622	15.98	0.800	3.548	465039.8	0.092	0.907	0.074
5-5A2	5760	15689.88	300	4.435	70510.33	0.2	3.544	4.49	0.860	3.498	454777.6	0.099	0.937	0.046
5-5A1	7430	56516.07	350	4.461	93251.52	0.176	3.559	1.65	0.681	3.506	457914.4	0.098	0.955	0.053

Table 3.3: Wafer cleaned with Process II and annealed only once

Sample	Thickness	Ratio Al(200)/Al(	Anneal Temp	Al(200) Dtheta	Al(200) Intensity (Cts/sec)	Al(200) FWHM	Al(111) Dtheta	Al(111) Intensity (Cts/sec)	Al(111) FWHM	Si(111) Dtheta	Si(111) Intensity (Cts/sec)	Si(111) FWHM
6-1a1	1840	34.42	RT	4.311	4233.160	0.571	3.777	122.981	1.378	3.25	456828.9	0.101
		41.63	250	4.226	5099.144	0.524	3.703	122.481	1.300	3.239	460478	0.097
		62.98	300	4.262	4416.990	0.489	3.705	70.131	1.315	3.249	453041	0.098
		61.52	350	4.23	3771.09	0.511	3.692	61.302	1.308	3.234	463307	0.1
6-1a2	2061	33.43	250	4.211	5076.308	0.553	3.735	151.852	1.344	3.231	460689.6	0.095
6-3a1	200	5.81	RT	4.188	24.45	1.3	3.465	4.21	2.574	3.244	446808.4	0.103

Table 3.1: XRD measurements of wafer cleaned with Process I

Sample	RBS Thickness (A)	Anneal Temp (C)	Al(200) 2theta	Al(111) 2theta
5-1b4	2280	RT	44.751	38.490
		200	44.794	38.509
		250	44.839	38.535
		300	44.849	38.493
		350	44.849	38.300
5-2a4	42	RT	44.783	38.268
		200	44.830	38.481
		250	44.768	38.421
		300	44.914	38.410
		350	44.938	38.392
5-4a4	266	RT	44.787	38.498
		200	44.835	38.546
		250	44.867	38.489
		300	44.907	38.541
		350	44.978	38.569
5-5a4	3540	RT	44.742	38.478
		200	44.778	38.488
		250	44.815	38.482
		300	44.853	38.357
		350	44.851	38.471

Table 3.5: 2θ values of Al(100) and Al(111)

CHAPTER 4

DISCUSSION OF RESULTS

4.1 RBS Data

RBS data were used to determine the thickness of the samples which were cut from the various parts of the wafers. As Table 3.1 indicates, the thickness measured by RBS is very different from the thickness measured by the quartz monitor. This is due to the variation of the aluminum flux from the source with angle and the misalignment between the vapor shield sector hole, and the quartz monitor.

For physical vapor deposition, the vapor flux from a plane source can be approximated by the $\cos^n \theta$ function where n is an integer and θ is the angle shown in the insert of Figure 4.1 [11]. In Figure 4.1, a plot of the cosine function with n=4 and n=29 was made with the plot of the film thickness measured along the wafer radius. The function $\cos^4 \theta$ describes the thickness distribution on a planar substrate where a disk vapor source is used [11]. Clearly, the thickness distribution is more like the $\cos^{29} \theta$ function than of the $\cos^4 \theta$ function.

The high value of n means that the vapor flux is highly directed. This highly directed flux is caused by the collimation of aluminum vapor by the cylindrical crucible. This highly directed beam coupled with the misalign-

ment of the source with the sector hole explains the big variation in the thickness distribution of the deposited films.

A few RBS channeling tests were performed on Sample 4-4. In channeling measurements a figure of merit, called minimum yield χ_{min}, is the ratio of the intensities between random and channeling (aligned) orientations [4]. The χ_{min} for Sample 4-4, channeling on aluminum, is 0.20 (Figure 3.2).

In this study, due to time constraints, channeling was considered to be a supplementary measurement.

4.2 XRD Data

The bulk of the measurements done in this study was performed using a x-ray diffractometer. The XRD technique provided a number of parameters which helped describe the Al/Si system. These parameters are outlined in detail below.

The 2θ value, using Bragg's Law, determines the interplanar spacing d, of the film. Knowing the interplanar spacing, the condition of the film (i.e. strained or relaxed) can be determined.

The θ value from the θ-scan determines the orientation of the scattering plane. This is important, because the scattering plane may not be parallel to the surface of the sample holder. In a diffractometer the angle θ is measured with respect to the plane of the instrument sample holder. There may be also be an offset in the θ scans due to the fact that the sample is not perfectly

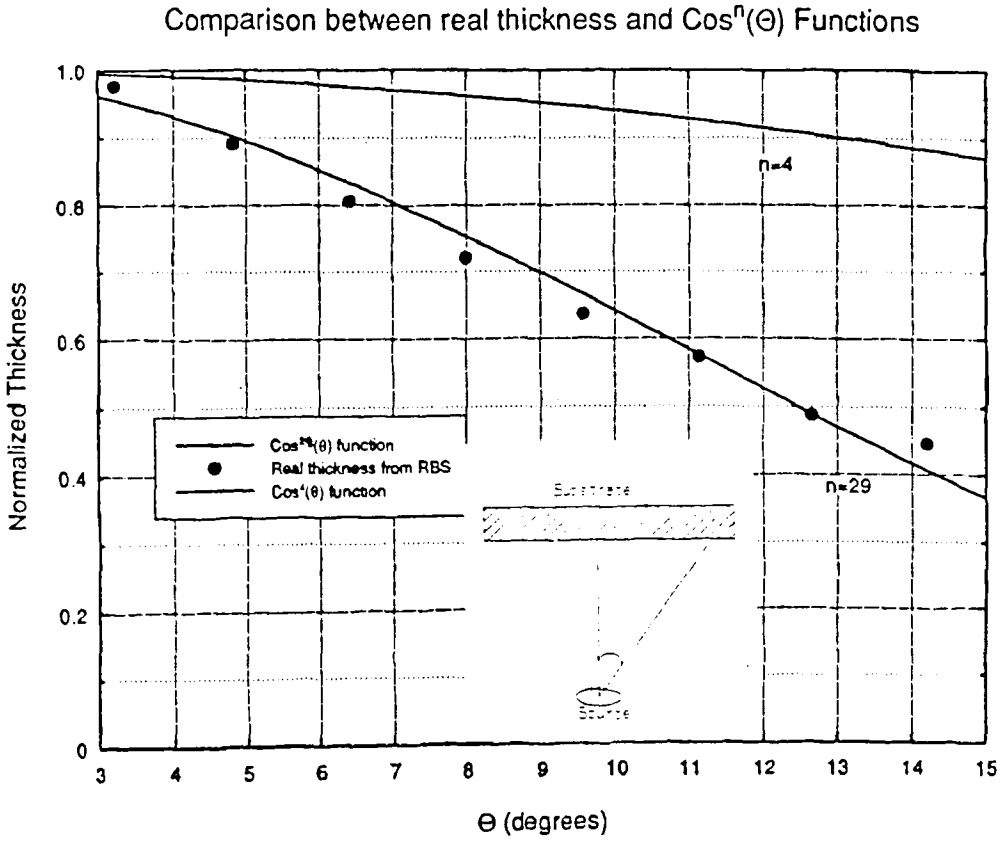

Figure 4.1: Comparison between RBS measured thickness and the $\cos^n \theta$ function

parallel to the sample holder because for example of the vacuum grease used to hold the sample. However, this error is not very critical because for each sample tested, θ scans of Si(111) and Al films were done one after the other without removing the sample from the holder. Therefore, measurements of θ with respect to the [111] direction of silicon crystal is insensitive to the misalignment of the substrate surface with respect to the sample holder. The value of θ for Al(200) and Al(111) with respect to Si[111] orientation are given in the last two columns of Tables 3.2.

The other parameter which is used to describe the quality of epitaxy is θ_{FWHM}. θ_{FWHM} determines the "mosaic spread" of the thin film crystal. If the film consists of crystals arranged in "tile-like" fashion, theirslight misalignment will result in broadening of the peak in the θ scans.

The θ_{FWHM} of Si peak is a measure of the overall resolution of the diffractometer since it can be assumed that the silicon substrate is a "perfect" single crystal. The value θ_{FWHM} of silicon can be used as the standard in quantifying the quality of the deposited films.

A striking feature of all the measured XRD spectra is that the Al(200) peak is very narrow and that the intensity of Al(200) peak is much larger than that of the Al(111) peak. This means that the film consists of very well aligned Al(200) crystals with only a small fraction of aluminum with (111) orientation. This contradict most data found in literature which reports that the (111) orientation as the most predominant orientation in aluminum films

deposited on silicon [10].

The ratio of the intensity of Al(200) to Al(111) is higher for films deposited on wafers cleaned with Process II compared to the ratio of Al(200) to Al(111) on films deposited on wafers cleaned with Process I.

An analysis of data in Table 3.3 showed that the orientations of the different planes have the vector configuration shown in Figure 4.2.

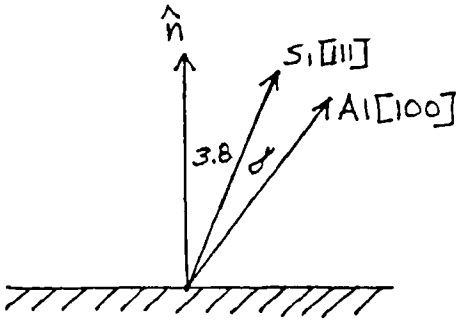

Figure 4.2: Vector notation of the different planes of the film

In Figure 4.2 $\hat{n}$ is the vector normal to the surface of the sample which is at an angle of 3.8° to Si[111]. This angle, which is sometimes called the "miscut" of the wafer is obtained by averaging the values of Dtheta of Si(111) in Table 3.2. α is the average of the angles dt-dtsi for Al(200) for different annealing temperatures in Table 3.5.

The interesting aspect of the vector configuration is that the Al[100] vector is in the Si[111] and $\hat{n}$ plane. Figure 4.3 shows the same vectors together with the different crystallographic axes of silicon. This relation between vectors shown in Figure 4.3 were obtained with the help of Dr. Robert Fleming

of AT&T Bell Laboratories at Murray Hill using a diffractometer with high intensity x-ray source and many angular degrees of freedom.

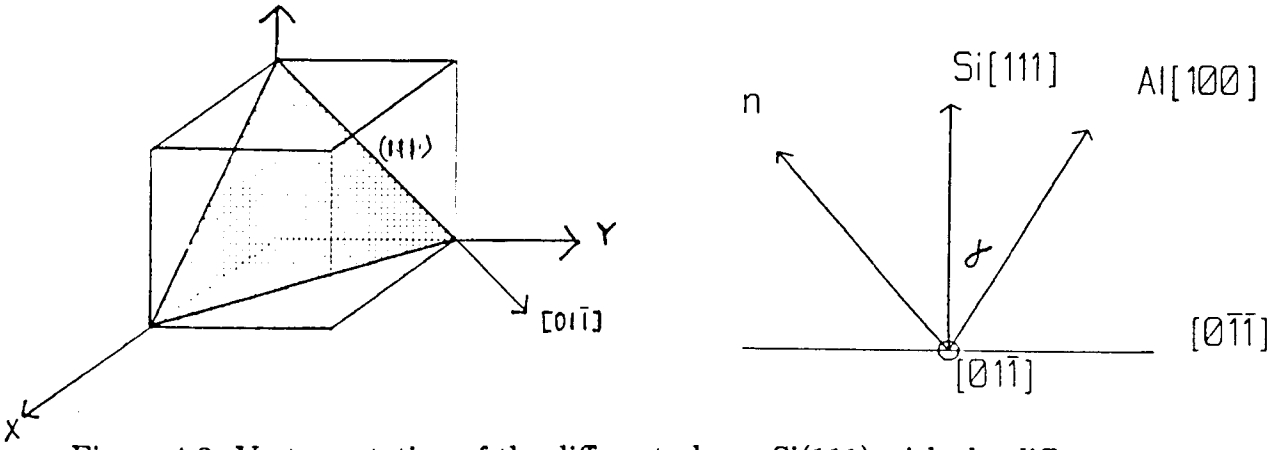

Figure 4.3: Vector notation of the different planes Si(111) with the different axes labeled

Based on the facts that the Al(200) peaks in XRD spectra are very narrow and that the Al[100] vector is not normal to the substrate plane and also at the same time in the Si[111] and $\hat{n}$ plane, we can conclude that the deposited films can not consists of domains with different rotational orientations but appear to be single crystals. Random rotational orientations would produce a spread in angle θ comparable to the tilt of Al[100] planes with respect to the surface.

The relationship between the film thickness and x-ray intensity of Al(200) is approximately linear as can be seen from Figure 4.8. This means that the x-ray intensity is roughly proportional to amount of aluminum present and the height of a peak corresponds to the amount of the material with that orientation in the film.

From Figure 4.7 it is clear that the ratio of intensity of Al(200) to Al(111) is larger for thicker films and increases after annealing. However, at certain temperature the ratio decreases and the θ_{FWHM} widens. This critical temperature seems to be related to the thickness of the film.

The very thin aluminum films have very small ratio of Al(200) to Al(111) because it may be that at the start of epitaxy there are many different crystal orientations. However, as the films grow a predominant orientation takes over.

Table 3.5 shows that 2θ value of the films deposited on wafer 5 changed slightly by $\sim .2^{\circ}$ after annealing. Figure 4.10 shows the effect of annealing on the average value of 2θ and to the interplanar spacing.

Figure 4.9 shows the relationship between the average α and the annealing temperature. Figure 4.9 clearly shows that θ_{FWHM} was reduced at even a low temperature (250°C) annealing. However, any subsequent annealing at higher temperature did not decrease the value of θ_{FWHM} any further. The observed changes of θ and 2θ of Al(200) are very small compared to the angular resolution of the diffractometer. Systematic changes with annealing temperature however, suggest that they are real.

The fact that Al[100] vector is in that plane is very important because this could explain the observed epitaxy of Al(100) on Si(111). The explanation of Al(100) epitaxy on Si(111) is given below:

After the chemical treatment of the wafers using Process II described

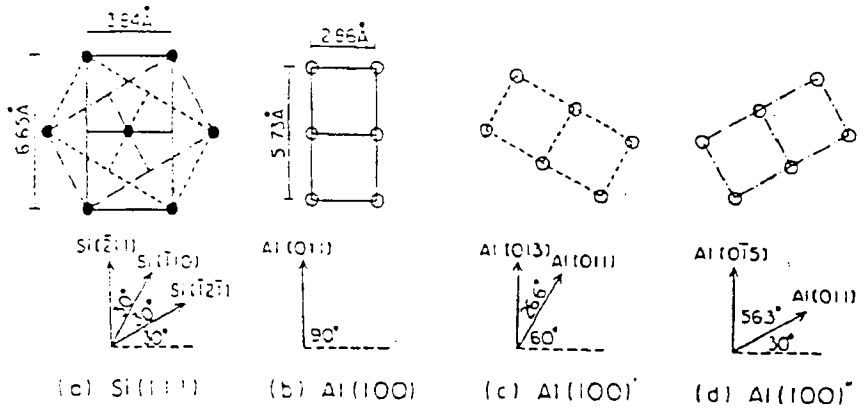

Figure 4.4: Illustration of the three possible orientations of Al(100) on Si(111) surface

in Section 2.3, atomic steps which are uniform and evenly distributed are formed in the surface of Si(111) wafer [7] (see Figure below). This steps which run perpendicular to the plane of Si[111] and $\hat{n}$ vectors serve to align the Al(200) structure. The steps are the preferred site of nucleation because they are the sites of the least energy for aluminum atoms on the substrate surface. Without the steps the Al(100) structure can have three different orientations on a flat Si(111) surface as shown in Figure 4.4 reference [8]. The film consisting of domains with different rotational orientations could not form a single crystal. With the steps serving as a guide, islands with the preferred orientations will predominate and therefore a single crystals may be grown as observed.

4.3 TEM Data

The Atomic resolution TEM image shown in Figure 4.11 clearly shows that the deposited aluminum film is good quality. The atomic steps and the miscut are clearly seen in the Si-Al interface.

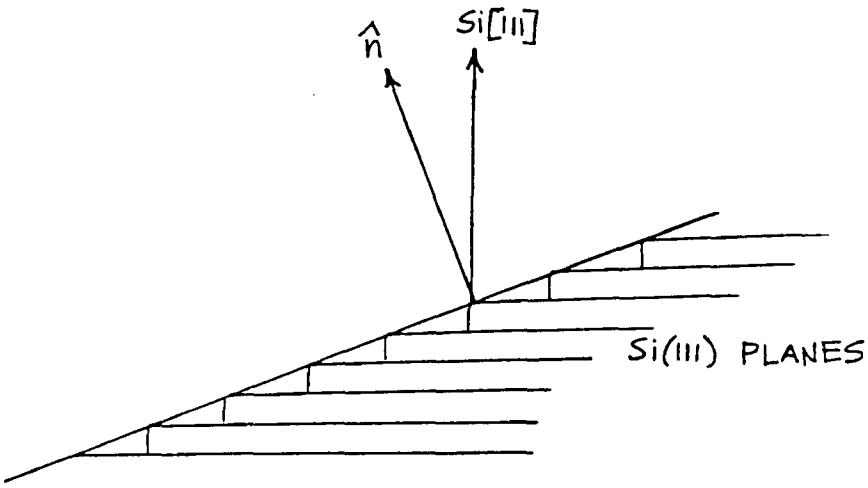

Figure 4.5: Schematic diagram of the steps on the Si(111) surface

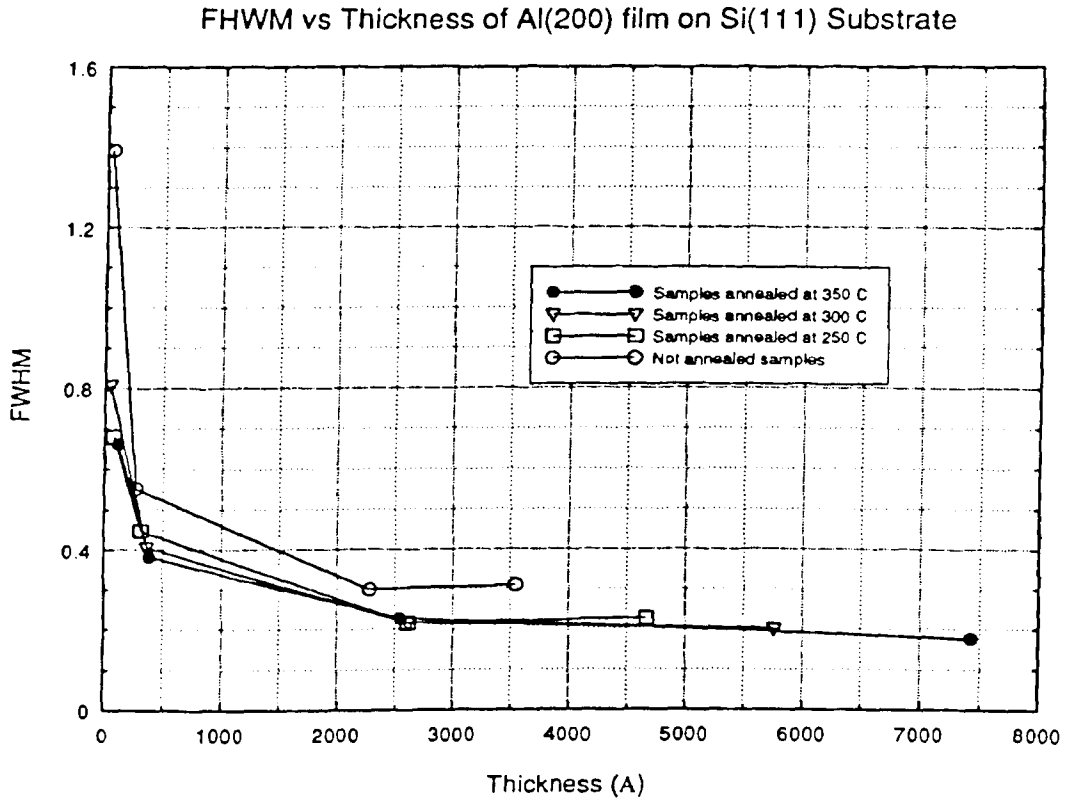

Figure 4.6: FWHM vs thickness of Al(200) film for various annealing temperature

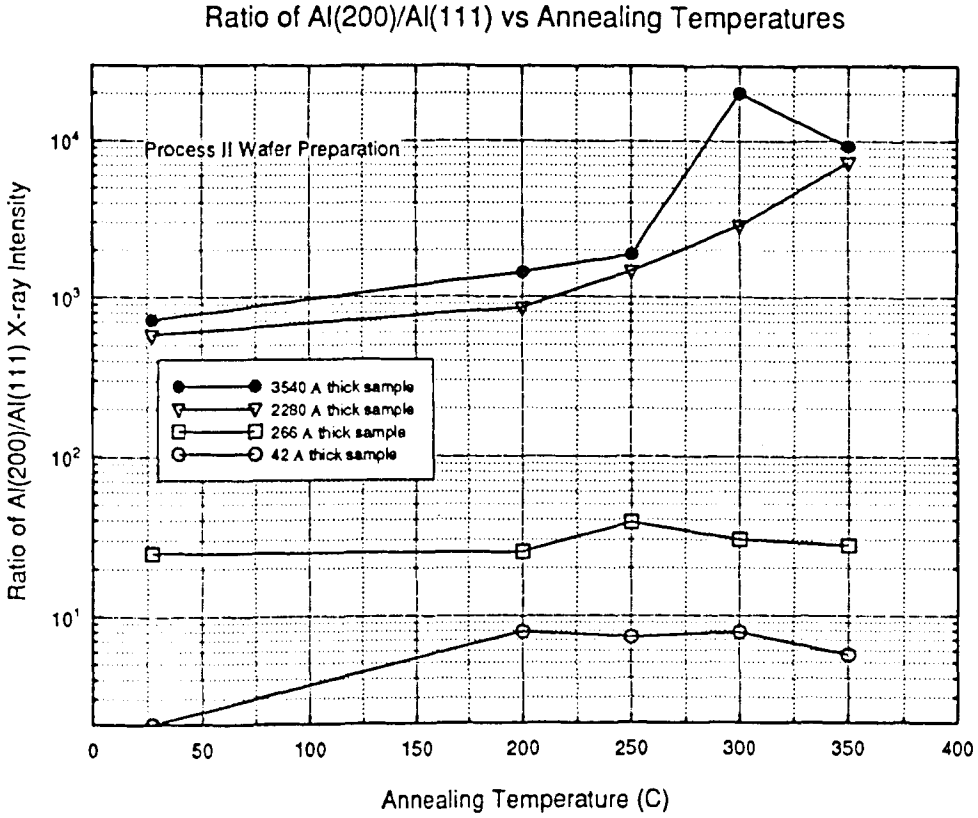

Figure 4.7: Ratio of Al(200) to Al(111) intensity vs annealing temperatures

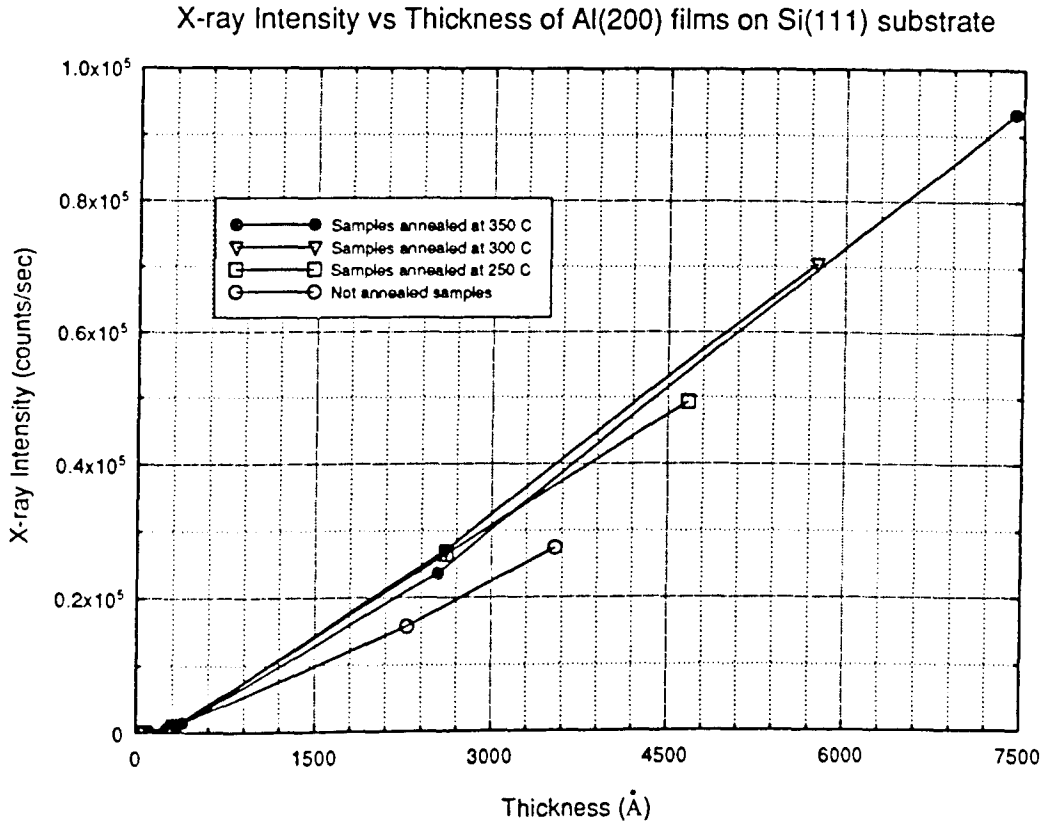

Figure 4.8: X-ray intensity vs thickness of Al(200)

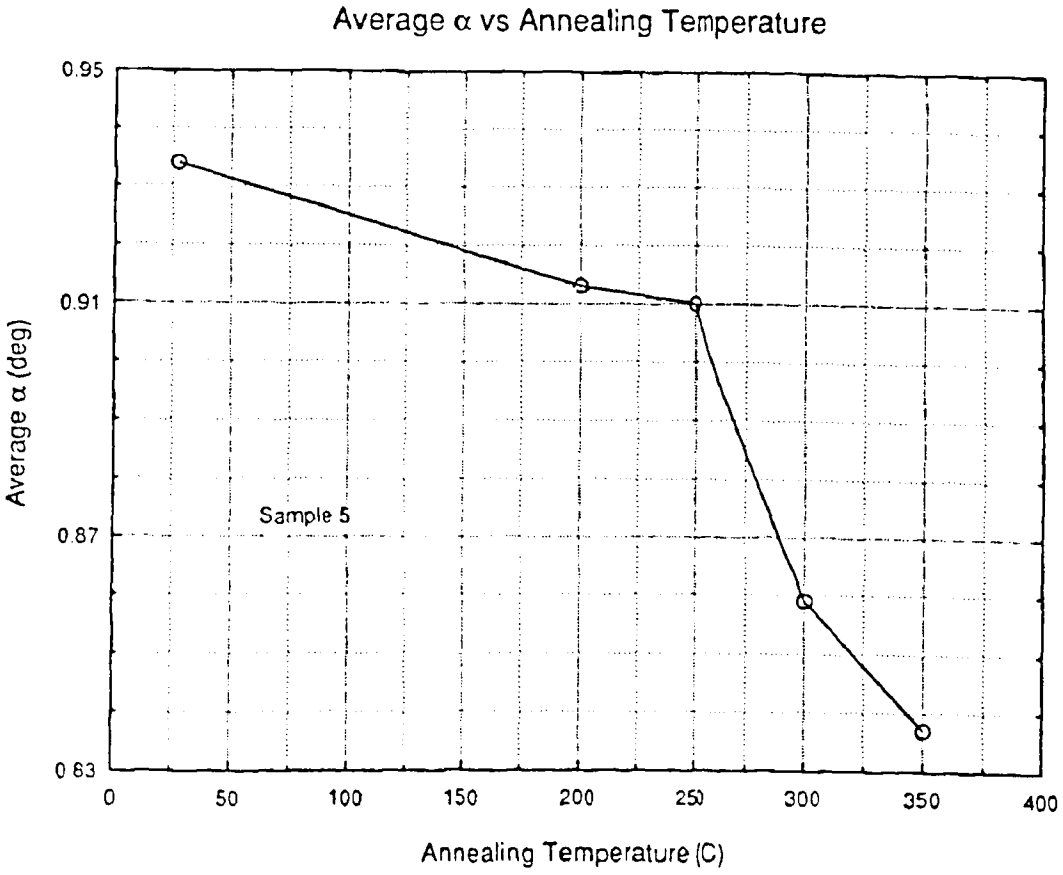

Figure 4.9: Average α versus annealing temperatures

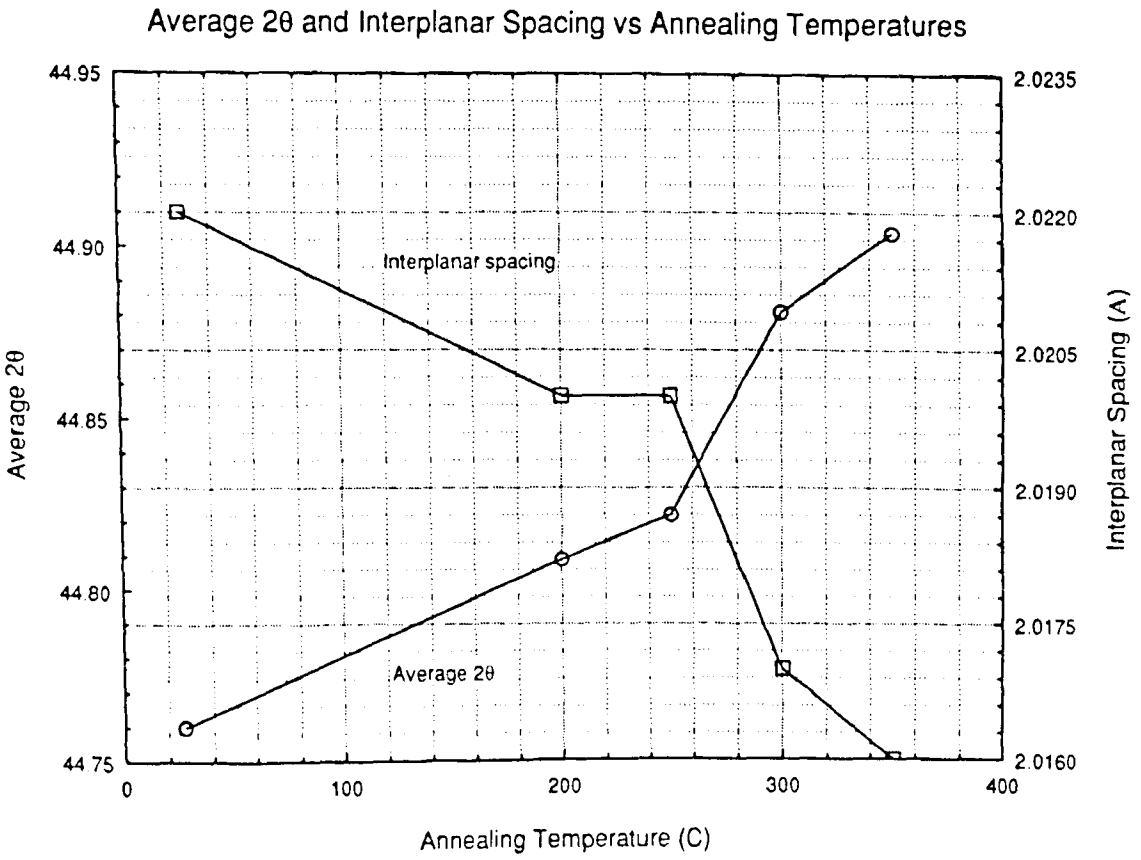

Figure 4.10: Average 2θ and interplanar spacing vs annealing temperatures

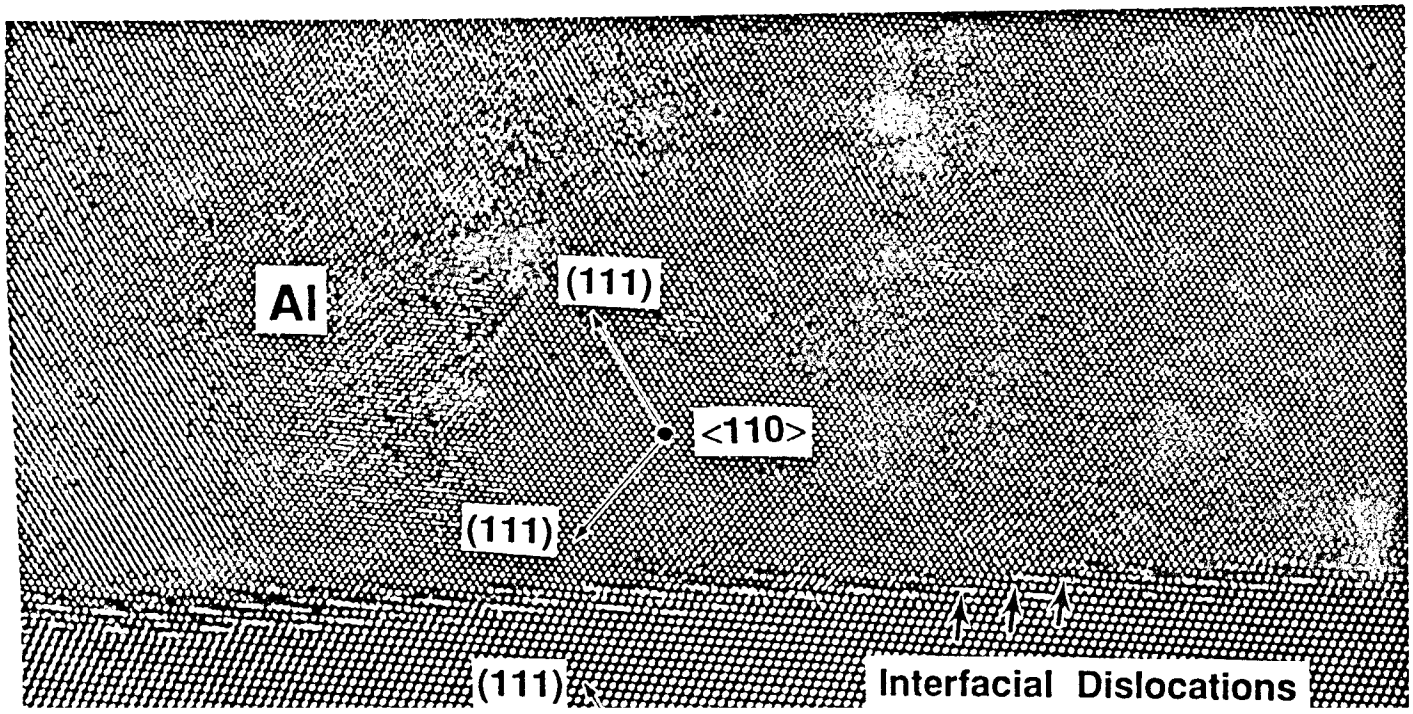
Al
(111)
<110>
(111)
(111)
Interfacial Dislocations

CHAPTER 5

SUMMARY OF RESEARCH FINDINGS

Pure aluminum was deposited on Si(111) substrates on room temperature, by thermal evaporation under ultrahigh vacuum ($\sim 10^{-9}$). The Si(111) surface was inclined from the normal to the substrate surface. Prior to depositions, clean silicon surface was hydrogenated by treatment in HF or HF and NH_4F solutions [7].

The XRD measurements showed that the deposited aluminum films had (200) orientation with only a small fraction of the film in Al(111) orientation. This fact contradicts a number of publications which report Al(111) films on Si(111) surface [3] [12] [2].

The ratio of the x-ray intensity of Al(200) to Al(111) peaks was 581 for films deposited on wafers prepared using both HF and NH_4F, and 34 on wafers treated with HF only.

Annealing in vacuum at 250°C increased the above ratio to 1472 and 42 respectively. The ratio of Al(200) to Al(111) intensities is larger in thick films than in thin films.

The detailed analysis of the XRD data showed that the Al[100] vector is at $\sim 1°$ with respect to the Si[111] and $\sim 4.5°$ with respect to the surface normal and vectors are in one plane. These findings led to the conclusion that the Al(100) films grew epitaxially in Si(111) and appears to be single

crystal. High quality of the Al(100) film was confirmed also by the RBS channeling experiments.

The epitaxial growth of Al on Si(111) can be explained by the presence of the atomic steps on the Si(111) surface. These uniform and evenly distributed steps, according to Higashi et al. were formed by the HF and NH_4F chemical treatment [7]. This steps on the silicon surface serves as the sites of nucleation.

The results and their interpretations were supported by the Transmission Electron Microscopy (TEM) images obtained with atomic resolution at Bell Laboratories. The images show abrupt Al-Si interface with visible atomic steps.

The results of this study should enhance the understanding of epitaxy between materials with large lattice mismatch.

An important area of research where our findings can be significant is in electromigration studies. Being able to grow epitaxial films of pure aluminum is highly desirable in the study of electromigration phenomena which depends on crystallographic structure of the materials [5].

BIBLIOGRAPHY

[1] Cullity B.D. *Elements of X-Ray Diffraction.* Addison Wesley, 2nd edition, 1978.

[2] Yapsir A.S., Choi C.H., and Lu T.M. Observation of a new Al(111)/Si(111) orientational epitaxy. *Journal of Applied Physics*, 67:796–799, 1990.

[3] Yapsir A.S., Lu T.M., Choi C.H., and Harper R.A. Epitaxial growth of Al(111)/Si(111) films using partially ionized beam deposition. *Applied Physics Letters*, 51:1992–1994, 1987.

[4] Mayer J.W., Chu W.K., and Nicolet M.A. *Backscattering Spectrometry.* Academic Press, 1978.

[5] D'Heurle F.M. and Ames I. Electromigration in single-crystal aluminum films. *Applied Physics Letters*, 16:80–81, 1970.

[6] Radnoczi G., Hansson G.V., Hasan M.A., and Sundgren J.E. Epitaxial growth of Al by thermal evaporation in UHV: Growth on Si(100)2x1 single & double domain surfaces at room temperature. *Surface Science*, 1990.

[7] Chabal Y.J., Becker A.J. Higashi G.S., and Becker R.S. Comparison of Si(111) surfaces prepared using aqueous solutions of NH_4F versus HF. *Applied Physics Letters*, 58:1656–1658, 1991.

[8] Yamada I. *MRS Symposium Proceedings*, volume 128. Material Research Society, 1988.

[9] Black J.R. *Proceedings of the 6th International Reliability Physics Symposium.* IEEE, 1968.

[10] Krakow W., Ho P.S., and Legoues, F.K. Atomic structure of the epitaxial Al-Si interface. *Philosophical Magazine*, 53:833–841, 1985.

[11] Ohring M. *The Materials Science of Thin Films.* Academic Press, 1992.

[12] Fujieda S., Miura Y., and Hirose K. Single-crystal Al growth on Si(111) by low-temperature molecular beam epitaxy. *Applied Physics Letters*, 62:1751–1753, 1993.

[13] Sze S.M. *Semiconductor Devices: Physics and Technology.* John Wiley & Sons, 1985.

[14] Sze S.M., editor. *VLSI Technology.* McGraw Hill, 2nd edition, 1988.

[15] Yamada. Epitaxial growth of Al on Si(111) by ionized-cluster beam. *Journal of Applied Physics*, 56:2746–2750, 1984.